THE ASTRONOMICAL JOURNAL VOLUME 84, NUMBER 6 JUNE 1979

DYNAMICAL STUDIES OF GLOBULAR CLUSTERS BASED ON PHOTOELECTRIC RADIAL VELOCITIES OF INDIVIDUAL STARS. I. M3

JAMES E. GUNN
Hale Observatories, California Institute of Technology, Carnegie Institution of Washington, Pasadena, California 91125

R. F. GRIFFIN[a)]
Cambridge Observatories, Cambridge CB3 0HA, England
Received 24 October 1978; revised 8 March 1979

ABSTRACT

Velocities of 111 stars in the globular cluster M3 have been measured using the Palomar cross-correlation radial-velocity spectrometer. Typical measuring accuracy is ~ 1 km s^{-1}. No velocity variation in nonpulsating stars is found; the implication that the incidence of binarism with separations in the range 0.3–10 AU is very much smaller than in the population I field is clear. "Thermal equilibrium" models of the King–Mitchie type with several components and anisotropic velocity distributions are constructed and found to represent the cluster dynamics and observed light distribution adequately. The existence of two very-high-velocity objects and some difficulty with the Roche limit indicate that the thermal equilibrium models do not describe the high-energy end of the distribution function adequately. There is no evidence for any very heavy remnants, and no mass that is not accounted for by evolution of the adopted mass function (which is steeper than the solar neighborhood one).

I. INTRODUCTION

The striking visual appearance of globular star clusters naturally arouses much interest in the dynamical state of these objects, the modeling of which has been a favorite pastime for theorists for many years. Since the subject passed out of the realm of pure speculation at the end of the last century with the discussion of star counts in clusters by Pickering (1897), many authors have contributed to the problem and not a few to its solution. Among them we may mention von Zeipel (1908), Plummer, (1911, 1915), Jeans (1916), Spitzer (1940) and his collaborators (Spitzer and Härm 1958; Ostriker, Spitzer, and Chevalier 1972), Camm (1952), Woolley (1954) and his collaborators (Woolley and Robertson 1956; Woolley and Dickens 1961, 1962), von Hoerner (1957), Oort and van Herk (1959), King (1962, 1966), Mitchie (1963), Mitchie and Bodenheimer (1963), Lohmann (1963, 1975), Petersen and King (1975), and Da Costa and Freeman (1976).

The first models with a realistic distribution function were probably those of King (1966), who summarizes and gives references to previous work. King's models use only one component and have isotropic velocity distributions, but the generalizations to models with stars of different masses and with possible anisotropy (Mitchie 1963) is in principle straightforward. The work of Da Costa and Freeman (1976) on M3, which we also study in this paper, is probably the most careful modern treatment using King's methods, although again only isotropic distribution functions are considered.

A major stumbling block to all such efforts has been the absence of dynamical data: The observational inputs to all the discussions mentioned have consisted, at most, of star counts and luminosity distributions. Although in some cases (Oort and van Herk 1959; Lohmann 1963, 1975; Petersen and King 1975) deductions have been made as to the velocity dispersions within individual globular clusters, actual measurements of the internal kinematics of clusters have been singularly lacking. The reason is that the dispersions in both the proper motions and in the radial velocities of individual member stars have been too small to measure reliably. Proper motions, even in favorable cases, can only amount to a few ten-thousandths of a second of arc per annum, while radial-velocity measurements of the necessary accuracy have not been possible for stars of such faint apparent magnitudes as those of even the brightest members of globular clusters until very recently. Recently Cudworth (1976) has succeeded in treating globular cluster proper motions in a semistatistical fashion. Popper (1947) and Joy (1949), who were among the first to obtain spectrograms of globular-cluster stars, specifically stated that the radial velocities measured from their plates were not good enough to permit discussion of the velocity dispersions of the clusters concerned. Deliberate efforts have been made to obtain the velocity dispersions in M92 (Wilson and Coffeen 1954), 47 Tuc (Feast and Thackeray 1960), and ω Cen (Harding 1965), but in each the observed dispersion was so close to the spread expected from errors of measurement alone that an upper limit to

[a)]Guest Investigator at the Hale Observatories.

 0004-6256/79/060752-22$00.90

the true dispersion was the only reliable result. Harding (1965) did, however, show that the mean velocities of two groups of stars, chosen on opposite edges of ω Cen in accordance with a preconceived hypothesis of rotation, differed significantly from one another. Illingworth (1976) has used spectrograms of the integrated light of the cores of a number of globular clusters (not including M3) to obtain characteristic central velocity dispersions from the smearing of the spectra, and very recently Da Costa *et al.* (1977) have obtained spectra of 11 stars in the southern cluster NGC 6397 to sufficient accuracy to derive a dispersion.

A careful dynamical study of a cluster clearly requires the determination of accurate velocities for many stars at many radii, for the core to the far outer reaches of the cluster. It was primarily for that task that the Palomar radial-velocity spectrometer (Griffin and Gunn 1974) was constructed. A single observation with that instrument is normally accurate to about 1 km s^{-1}, a quantity which is small in relation to the expected velocity dispersions in globular clusters; in rich clusters we can readily measure ~100 stars within practicable total observing times. We are, therefore, for the first time in a position to discuss not only the velocity dispersion but also the dynamical state of a globular cluster on the basis of reliable radial velocities of a substantial number of individual stars.

During the last seven years, the Palomar spectrometer has been used to determine velocities in several clusters, including M3, for which we have results on 111 stars; those are the data which we wish to discuss here. Rather more data exist for M13, which was the cluster we studied first, but owing to its rotation (Babcock 1971), it is more difficult to discuss and we defer it to a later paper in this series. Some few tens of velocities exist for each of the clusters M5, M10, M22, and M92, and a few in M15. These objects will also be discussed in later papers.

The data on M3 are presented and discussed in Sec. II along with a discussion of the errors of measurement and an additional, apparently astrophysical, random component that may be due to atmospheric motions in the high-luminosity giants whose velocities we obtain. We also present the evidence for a remarkable absence of binarism among globular-cluster stars.

In Sec. III the astrophysical input parameters are discussed, including the mass–luminosity relationship, the mass function, and the cluster distance modulus and age. The models, which include many stellar masses and anisotropy, are discussed in Sec. IV. Section V is partly pedagogical, and discusses a series of three-component models that illustrate the effects of varying the various mass and anisotropy parameters one has at one's disposal to fit the observational data.

Using the velocity data is not completely straightforward; an approximate maximum-likelihood technique for fitting the models to the observed velocities is discussed in Sec. VI, as is the adopted technique for fitting to the observed light distribution. A new test for assessing the goodness of fit for the velocities, which is applicable in general to testing for homogeneity of variance of nearly normal populations, is described.

Relaxation phenomena are explored in Sec. VII; it is there shown that our assumption of a mass-independent anisotropy radius is at least reasonable and that the assumption of thermal equilibrium is somewhat questionable. The existence of two very-high-velocity stars in M3 is discussed, and their origin and fate considered.

Section VIII deals with the model fit to M3 and discusses some of the problems with which one must contend and the tradeoffs which can be made. Difficulties with the mass-to-light ratio, with the necessity for introducing velocity anisotropy, and with the inferred maximum extent of the cluster are discussed.

Section XI is a summary and general discussion.

II. OBSERVATIONS

Stars in M3 were observed in the course of observing runs on the Hale 5-m telescope in the years 1972–1976. Integration times rarely exceeded 15–20 min, and the choice of stars for measurement was correspondingly restricted to those brighter than about $V = 14.0$ mag. Most stars brighter than 14 mag in the vicinity of the cluster were observed; the total number was 122, of which 111 proved to have radial velocities sufficiently close to the mean velocity of the cluster to carry a strong implication of membership, the mean velocity being high enough (−147 km s^{-1}) to make contamination by field stars very unlikely. It is presumed that red stars [$(B - V) > 0.6$ mag] that gave no result when we observed them have velocities lying outside the range of our scan and are therefore nonmembers; stars of unknown color could also fail to give a result through being of too early spectral types.

Photoelectric velocities have to be measured differentially against a standard. The standard needs to be a star in the first instance; an emission source can also be used as an intermediate standard in a number of different ways, one of which is outlined in our earlier paper (Griffin and Gunn 1974). For several reasons the standard star should have a radial velocity close to that of the cluster, and should be near to it in the sky; it also ought to be bright enough to give a very good radial-velocity trace in a short integration time, and be of such a spectral type as to give a deep "dip" on the trace to facilitate accurate measurement. The choice of standard stars is greatly restricted by the high velocities of many globular clusters (including M3), and a degree of compromise among the various criteria is almost inevitable. The star selected as a standard for M3 is HD 126778; its angular distance from the cluster is about 10°, and its magnitude and spectral type are 8.18 mag and K0 III, respectively (Roman 1955). The radial velocity of the standard star, discovered to be large by Heard (1956), who obtained

a value of -130.1 km s^{-1}, has been kept under review during the period covered by the M3 observations by occasional photoelectric observations both with the Palomar instrument itself and with the original Cambridge spectrometer (Griffin 1967). In these observations its velocity has been compared directly with that of the primary photoelectric reference star 41 Com (Griffin 1967); the results are given in Table I. We do not consider that there is any evidence for variation in the velocity of HD 126778—a conclusion reinforced by the mutual agreement of the zero points derived from the star and from helium lines (Griffin and Gunn 1974) in different observing seasons—and in this respect we have been favored by fortune, as we had little prior evidence that the velocity of our reference star was constant. There is no significant difference between the velocities obtained with the two telescopes either, and we adopt for the velocity of HD 126778 a straight mean of the measurements in Table I, viz. -137.3 km s^{-1}, the standard error of the mean being 0.25 km s^{-1}. [The large velocity difference to be spanned between 41 Com and HD 126778 involves the possibility of additional nonrandom errors due to "mismatch" (Griffin 1967), but they are not expected to be as large as 0.25 km s^{-1} in the present case.] On this basis the mean velocity of M3 stars is -146.9 km s^{-1} and, for convenience, we refer all velocities in M3 to this cluster-mean velocity rather than to the velocity of the sun.

In Table II we present our observational results on M3, together with other relevant data on the stars concerned. The first column shows the number of the star as designated by von Zeipel (1908). To assist in cross identifying stars that later authors have rechristened, we give in column 2 the numbers given by Barnard (1931) in his astrometric study, made with a filar micrometer, of 147 stars in the central region of the cluster and in column 3 the quadrant, and also letter, designations of Sandage (1953). In the fourth and fifth columns are the m_{pv} magnitudes and the color index. Photoelectric magnitudes from Baum (1952), distinguished in the table by asterisks, are quoted where available; failing them, photographic magnitudes are given, and, in their absence—which is almost inevitable over the whole of the dense central region—Barnard's (1931) eye estimates are used. In most cases where a comparison is possible, Barnard's magnitudes are in good accord with modern determinations. The source of every magnitude is given; the key to the references is at the end of the table. Columns 6–8 give the appropriate coordinates and the radial separation of the star in seconds of arc from the cluster center, which Barnard took to be 13 arcsec south of von Zeipel 807. He gave this star's position as $13^h37^m35^s.13$, $+28°53'08''.0$ (1900). Von Zeipel (1908) found the position of the same star to be $13^h37^m35^s.27$, $+28°53'08''.2$. Barnard's coordinates are quoted for the stars in Barnard's catalog; for the other stars we have derived the coordinates from von Zeipel's right ascensions and declinations. Columns 9 and 10 show the dates and results of our radial-velocity measurements; the internal standard error in column 11 of each velocity has been computed from the statistics of the photon counts in individual "bins" of the trace in the manner described in our first paper (Griffin and Gunn 1974).

TABLE I. Photoelectric radial velocities of HD 126778.

Date	Velocity (km s^{-1})	Telescope[a]
14.90 July 1972	−137.7	36
18.97 May 1973	−137.9	36
11.15 June	−136.9	200
31.21 May 1974	−137.5	200
7.15 Mar 1975	−135.8	36
24.16 May	−138.0	200
7.95 June 1976	−137.4:	36
28.90 July	−136.9	36
30.23 Jan 1977	−137.7	36
16.02 Apr	−137.7	36

[a]36—Cambridge 0.92-m telescope (Griffin 1967); 200—Hale Telescope (Griffin and Gunn 1974).

In column 12 is the mean of the observed radial velocity measurements for each star, and in columns 13 and 14 are the values of χ^2 and the number of degrees of freedom associated with the stars that have more than one determination, using the computed standard error for each measurement.

The true errors of the observations may be assessed by intercomparing the results for those stars observed more than once. We reject immediately from this discussion two stars (vZ 318 and 803) that have long been known to be variable in light (Bailey 1913, Barnard 1906) and are already known to exhibit large variations in radial velocity (Joy 1940, 1949). They are a long-period variable and a W Virginis star, respectively. These are the only stars that show unambiguous evidence for velocity variation, and that variation comes about almost certainly as the result of pulsation.

With the exclusion of these two, the cumulative χ^2 is 86.2 for 43 degrees of freedom. The expected value is 43, of course, and the deviation is significant at the 0.01% level. The implication is that we have underestimated our errors or that there are larger systematic errors than we have thought. Other circumstances, however, make both these conclusions seem unlikely. In our study of the Hyades and of M67 we have attempted to observe a group of stars to high accuracy, of order 300 m s^{-1}. We have had no difficulty maintaining this sort of stability from run to run, and no special precautions have been taken that we do not routinely take for the globular cluster observations as well; in addition, the predicted errors seem to represent the velocity spread quite well. It is also striking that the velocity spread in the M3 stars seems not to depend very much on the calculated errors—i.e., the values of χ^2 are largest in those cases in which the individual measurements are quite good formally. This situation suggests that an *additive* error is the culprit, and we suggest for the above-mentioned reasons that its origin is not instrumental but astro-

TABLE II. Photoelectric radial-velocity observations of individual stars in M3.

Star identification Von Z	B	S	Magnitude m_{pv}	C.I.	From cluster center x	y	r	Radial-velocity observations Date	r.v. km/s	s.e. km/s	Mean r.v. km/s	χ^2	ν
98					-1025	+18	1025	1974 June 3.27	No result		—		
115					-903	+227	931	1974 June 1.21	+0.56	0.83	+1.35	1.63	1
								1976 July 7.23	+1.98	0.74			
129*			12.66*	0.47*	-803	+310	861	1974 June 1.20	No result		—		
164					-549	-19	549	1974 June 1.20	+5.69	0.85	+5.69		
177		IV-25	13.62*	1.06*	-469	-71	473	1974 June 1.19	-0.57	0.84	-0.57		
192		IV-27	14.03	0.88	-371	-16	371	1974 June 1.18	-1.01	1.17	-1.01		
194		AE	13.87*	0.98*	-361	+209	417	1974 June 1.22	-0.17	1.02	-0.17		
205		III-28	12.74	1.25	-342	+144	371	1972 May 23.20	-2.23	0.77	-3.98	12.87	1
								1976 July 7.19	-6.59	0.94			
206			9.86*	1.09*	-338	+282	440	1974 June 1.21	No result		—		
238	1	AA	12.63*	1.52*	-266	+46	270	1972 May 23.19	-2.79	0.79	-2.40	0.46	1
								1974 June 3.27	-2.05	0.75			
250		S	14.10	0.90	-245	-195	313	1973 June 9.26	-6.70	1.15	-6.70		
263	3	U	13.57*	1.05*	-227	-97	247	1973 June 9.25	-2.13	0.79	-2.13		
265		IV-101	13.31*	1.35*	-221	-202	300	1973 June 9.27	+1.70	1.07	+1.70		
281		AH	13.79	1.01	-202	+200	284	1972 May 23.21	-2.13	0.84	-2.13		
287					-191	-846	867	1974 June 3.20	+2.51	1.06	+2.90	0.21	1
								1976 July 8.26	+3.12	0.80			
291*	7		13.2		-186	-1	186	1974 June 1.17	-4.04	1.45	-4.04		
297			12.85*	1.40*	-181	-405	444	1973 June 9.27	-3.93	0.82	-3.09	2.19	1
								1976 July 7.22	-2.17	0.86			
309	9	III-64	13.16	1.21	-164	+20	165	1972 May 23.19	+4.66	0.87	+4.66		
318*	11		var		-158	+20	159	1972 May 23.18	-5.52	0.68	var		
								1973 Jan 15.52	+1.71	0.94			
								1974 May 29.17	-5.89	0.71			
								June 1.16	-6.94	0.84			
								3.17	-3.03	0.65			
								1975 May 24.17	-6.68	0.85			
								1976 July 7.20	-7.97	0.88			
333					-147	-714	729	1974 June 3.21	No result		—		
334	15	IV-77	13.27	1.13	-148	-60	160	1972 May 23.17	+1.10	0.86	+1.10		
345*	18	IV-82	13.51	1.26	-137	-118	181	1972 May 23.17	No result		—		
387	30		13.8		-109	+67	128	1974 June 1.24	-4.36	1.32	-4.36		
398	31	III-77	13.36	1.15	-103	+152	184	1972 May 23.22	+8.74	0.92	+7.52	2.82	1
								1976 July 8.24	+6.79	0.71			
417	32		13.6		-92	-32	97	1973 June 10.18	+7.26	1.23	+7.26		
420*	33		13.8		-90	-7	90	1974 June 3.26	+8.07	1.19	+6.48	3.26	1
								1975 May 24.31	+5.17	1.08			
463	36	III-80	13.28	1.06	-74	+121	142	1972 May 23.22	-4.85	0.86	-4.85		
490	39		12.8		-66	-101	120	1972 May 23.16	-4.20	0.53	-4.63	1.95	1
								1973 Jan 14.57	-5.46	0.73			
508	41		13.0		-61	+15	63	1973 Jan 14.54	-1.69	0.91	-1.44	0.10	1
								1974 June 3.25	-1.34	0.59			
509	42		13.3		-60	+21	64	1973 Jan 14.54	-6.77	1.25	-6.77		
528	44		13.4		-55	-72	91	1973 Jan 14.57	-10.41	1.27	-9.70	0.53	1
								1975 May 24.27	-9.21	1.05			
545	45		12.8		-51	+82	97	1972 May 22.17	+3.32	0.82	+3.79	0.80	1
								1976 July 8.24	+4.47	0.99			
549	46		12.8		-50	+47	69	1972 May 24.24	-4.01	0.95	-4.01		
555	47		13.1		-47	-24	53	1973 Jan 14.55	-5.10	0.88	-5.02	0.01	1
								1975 May 24.27	-4.97	0.74			
574	49		13.0		-43	+27	51	1973 Jan 14.53	-0.41	1.03	-0.41		
576	50		13.3		-43	-40	59	1973 Jan 14.56	-4.46	0.72	-6.01	9.60	2
								June 9.18	-7.35	0.70			
								1974 June 1.24	-6.33	1.16			
585	51		13.7		-41	+66	78	1974 June 3.28	-1.43	0.95	-1.43		
589	53		13.4		-39	-85	94	1972 May 22.28	+1.71	0.81	+1.71		
591	52		13.5		-40	-50	64	1973 Jan 14.56	-3.50	1.00	-3.50		
592					-39	-2	39	1973 Jan 14.55	-0.79	1.23	-3.12	4.06	2
								1975 May 24.29	-3.91	0.85			
								1976 July 8.22	-3.43	0.83			
610					-36	-10	37	1973 Jan 15.54	+2.77	0.90	+2.77		
612	54		13.0		-36	+70	79	1973 Jan 15.58	+3.72	0.71	+3.72		
618	55		13.3		-33	+58	67	1973 June 10.19	+1.84	1.01	+1.84		
622	56		13.7		-33	-78	85	1972 May 22.27	-9.22	0.92	-9.22		
640	57	A	13.31	1.20	-30	-164	167	1972 May 24.18	-2.96	1.04	-2.96		
647	58		13.9		-29	-33	44	1973 June 9.19	+11.30	0.78	+10.89	0.59	1
								1974 June 1.25	+10.41	0.85			
670	60		13.3		-25	-6	26	1973 Jan 15.53	+0.16	0.77	+0.55	0.54	1
								1976 July 8.23	+0.99	0.82			
672	62		13.2		-24	+27	36	1973 Jan 13.57	-3.89	0.74	-3.89		
673	61		13.6		-25	-31	40	1973 June 9.20	-12.41	0.71	-11.82	1.64	1
								1976 July 8.18	-11.00	0.84			
682	64				-23	-17	29	1973 Jan 15.54	+5.29	0.96	+5.29		

TABLE II. (Continued).

Star identification			Magnitude		From cluster center			Radial-velocity observations				Mean	χ^2	ν
Von Z	B	S	m_{pv}	C.I.	x	y	r	Date	r.v. km/s	s.e. km/s		r.v. km/s		
684	65		13.7		-23	-51	56	1973 June 9.21	-4.89	0.80		-4.89		
688	67		13.4		-22	+15	27	1973 Jan 15.53	-5.11	0.77		-5.11		
706	69		13.3		-18	+87	89	1972 May 24.23	+3.49	1.00		+3.49		
716	71		13.7		-17	+65	67	1974 June 1.26	+0.15	0.84		+0.15		
726	73		12.6		-14	-20	24	1973 Jan 13.56	-3.29	0.63		-3.29		
729	74		12.4		-14	+17	22	1973 Jan 13.56	-2.72	0.74		-2.72		
733	75		12.5		-13	+20	24	1973 Jan 13.56	-6.17	0.64		-6.17		
740*	76	B	13.60	0.50	-13	-213	213	1973 June 10.21	No result			—		
746	78		12.9		-11	+20	23	1973 Jan 15.52	+1.59	0.92		+1.59		
748	77		13.6		-11	-3	11	1974 June 3.24	+0.04	0.84		+0.04		
752	79		12.8		-11	+69	70	1972 May 23.23	+3.43	0.77		+4.18	2.41	1
								24.23	+5.34	0.96				
763	81		13.0		-9	-35	36	1973 Jan 13.55	-4.94	0.74		-4.38	1.63	1
								1974 June 1.31	-3.34	1.01				
764	82		13.7		-9	-18	20	1973 Jan 15.54	+16.81	0.77		+16.97	2.46	4
								June 9.21	+17.17	0.69				
								1974 June 3.24	+17.17	1.11				
								1975 May 24.25	+18.17	1.13				
								1976 July 8.19	+15.95	0.90				
779	86		13.2		-6	+38	38	1974 June 1.29	-4.31	0.79		-4.31		
790	88		13.5		-3	+3	4	1973 Jan 15.55	+3.01	0.85		+3.01		
796	90		13.9		-2	+1	2	1973 Jan 15.55	+2.28	1.04		+2.28		
803*	91		var		-1	-24	24	1973 Jan 13.54	+14.82	1.32		var		
								June 13.18	+3.22	1.10				
								1974 May 29.18	-4.09	0.90				
								June 3.21	+10.65	1.46				
								1975 May 24.18	No result					
								1976 July 8.18	No result					
807	92		12.4		0	+13	13	1972 May 22.25	+7.87	0.71		+7.65	0.22	1
								1976 July 7.18	+7.35	0.84				
835	96		13.2		+5	-78	78	1972 May 22.25	-2.09	0.74		-2.09		
837	97	II-46	12.72	1.46	+6	+229	229	1972 May 22.18	-3.75	0.75		-3.75		
849	98		13.9		+7	-12	14	1973 June 9.22	+7.71	1.06		+7.71		
853	99	V-41	13.80*	0.89*	+7	-240	240	1973 June 10.22	+1.59	1.48		+2.00	0.12	1
								1974 June 3.29	+2.22	1.09				
855	102		13.1		+8	+25	26	1973 Jan 13.57	+4.97	0.73		+4.97		
858	103		12.8		+8	-44	45	1972 May 23.26	+9.74	0.75		+9.99	0.35	1
								1975 May 24.19	+10.53	1.11				
859	104		12.7		+8	-41	42	1972 May 23.26	+4.32	0.54		+4.32		
860	105		13.0		+8	+32	33	1973 Jan 13.58	-0.82	0.71		-0.82		
871	106		13.8		+9	-62	63	1973 Jan 14.58	+6.63	1.03		+6.63		
874	107		13.9		+10	+5	11	1973 Jan 15.56	+3.85	1.05		+3.85		
885	110	V-80	13.50	0.99	+12	-116	117	1973 Jan 14.58	-0.33	1.02		-0.33		
887	109		13.3		+12	+8	14	1973 Jan 15.56	+1.53	0.78		+1.53		
893	112		12.8		+14	+12	18	1972 May 22.26	-0.66	0.80		-1.28	1.01	1
								1973 Jan 15.58	-1.71	0.67				
898	113		13.2		+15	+7	17	1973 Jan 15.57	-3.20	0.96		-3.20		
911	115		13.5		+18	+6	19	1973 Jan 15.57	-22.24	1.16		-22.89	0.99	3
								1974 June 1.27	-23.03	1.30				
								1975 May 24.24	-24.14	1.51				
								1976 July 8.20	-22.71	1.11				
917	117		13.2		+18	-12	22	1973 June 9.23	+3.03	0.99		+3.03		
925	120		13.3		+20	-167	168	1972 May 23.25	+2.53	0.69		+2.53		
928	121		13.5		+21	+2	21	1973 June 9.24	+8.41	1.11		+8.41		
964	124		13.9		+28	+2	28	1973 June 9.24	+0.46	0.79		+0.46		
972	123		13.7		+28	+58	64	1974 June 3.23	-5.56	1.06		-5.56		
976	125		14.0		+29	+6	30	1974 June 1.28	-1.31	0.84		-1.31		
1000	126		12.9		+35	+174	177	1972 May 22.18	-4.44	0.77		-4.44		
1008	127		13.1		+36	+26	44	1973 June 10.20	-6.61	1.07		-6.61		
1053	130		12.7		+45	+48	66	1972 May 24.19	+5.93	0.72		+6.79	3.05	1
								1974 June 3.22	+7.77	0.77				
1059	131		13.9		+47	+37	60	1974 June 1.31	+3.95	0.77		+3.95		
1082	132		14.0		+54	-41	68	1973 Jan 15.51	+1.45	1.51		+1.54	0.01	1
								1975 May 24.22	+1.61	1.34				
1100	134				+59	-39	71	1973 Jan 15.50	-8.81	0.92		-10.81	6.64	2
								June 13.19	-11.80	0.89				
								1975 May 24.20	-11.57	0.82				
1121	135		13.5		+67	-32	74	1972 May 24.16	+3.04	0.93		+3.04		
1127	136		12.7		+67	+70	97	1972 May 22.19	+2.09	0.95		+2.09		
1135	137		13.3		+71	-24	75	1972 May 22.22	-10.61	0.81		-10.85	0.18	1
								1973 June 10.18	-11.12	0.87				
1142	138		13.7		+74	+23	78	1974 June 1.30	+2.88	1.01		+2.88		
1203	139	I-76	13.29	1.18	+94	+126	157	1973 Jan 13.52	+1.24	0.66		+1.24		

TABLE II. (Continued).

Star identification			Magnitude		From cluster center			Radial-velocity observations			Mean	χ^2	ν
Von Z	B	S	m_{pv}	C.I.	x	y	r	Date	r.v. km/s	s.e. km/s	r.v. km/s		
1208	140		13.3		+99	+71	122	1973 Jan 13.03	-1.12	0.90	-1.12		
1214	141	I-108	13.30	1.20	+103	+29	107	1972 May 22.21	+5.66	1.13	+5.66		
1217	142	I-106	14.03	0.97	+106	+6	106	1973 Jan 15.51	+3.70	1.39	+3.70		
1219	143	I-109	12.70	1.35	+106	+36	112	1972 May 22.20	-0.07	0.97	+0.27	0.24	1
								1976 July 8.27	+0.59	0.93			
1224		I-81	13.86	0.96	+109	+133	172	1974 June 3.18	+9.26	1.24	+9.26		
1241	145		13		+120	+39	126	1974 June 1.32	-1.81	0.87	-1.81		
1257					+122	-925	933	1974 June 3.19	No result		—		
1270		II-18	14.18	0.70	+138	+363	388	1974 May 29.23	-1.91	1.55	-1.91		
1273	147	I-87	13.54	1.04	+138	+88	164	1973 Jan 13.52	+3.19	0.69	+3.19		
1274		I-92	14.69	0.64	+139	+65	154	1973 Jan 13.50	+11.85	1.70	+11.85		
1345		BC	13.97	0.95	+227	+98	247	1973 June 9.29	-5.95	0.89	-5.95		
1360		I-46	13.89	1.00	+260	+15	260	1972 May 23.27	+0.64	0.86	+0.64		
1362		AV	14.12	0.88	+269	+264	377	1974 May 29.21	-4.99	1.06	-4.99		
1375					+310	-666	735	1973 June 9.28	No result		—		
1376		BF	13.67*	1.07*	+314	-161	353	1974 May 29.20	-2.78	0.96	-2.78		
1383		BI	14.11	0.90	+340	-362	497	1972 May 23.24	-2.42	1.62	-2.42		
1392		I-21	13.05*	1.28*	+365	+318	484	1973 Jan 13.54	+1.51	0.62	+1.49	0.00	1
								1976 July 7.22	+1.44	0.89			
1397			12.67*	1.57*	+393	-211	446	1972 May 23.24	+1.07	0.55	-0.23	13.34	1
								1976 July 7.21	-2.04	0.65			
1402*			12.67*	0.48*	+421	-402	582	1972 May 23.24	No result		—		
1446					+666	-342	749	1973 June 9.28	No result		—		
1449					+685	+21	685	1973 June 9.28	-3.38	0.83	-2.27	10.24	3
								1974 May 29.19	+0.19	0.89			
								1975 May 24.32	-3.00	0.77			
								1976 July 7.20	-2.49	0.92			
1469					+857	+296	907	1973 June 9.28	No result		—		

physical: motions in the atmospheres of these very luminous, low-mass stars, either of convective or pulsational origin, of very low amplitude are sufficient to account for the errors. In any case, a randomly additive "jitter" of 0.8 km s^{-1} rms brings χ^2 down to 43, and we henceforth will include this component in the error of a single measurement relative to the true radial velocity of a star. For the consideration of the dynamics, of course, its origin is of no consequence, so long as it is included properly in the computation of the true velocity dispersions.

One is immediately struck by the absence of large velocity variations; in our work on field giants, we find that about 30% of the stars are variable on the relevant amplitudes (few kilometers per second) and time (few years) scales. The large body of data on other globular clusters supports the tentative conclusion that binarism involving stars of not-too-disparate masses and separations between the radius of the giants (0.3 AU, say) and about 10 AU is either very rare or absent in globular clusters, in stark contrast to the situation in the solar neighborhood. Binaries in this mass range are "hard" enough that they are unlikely to interact significantly dynamically with the other stars in the cluster, though more widely separated ones can be disrupted (Hills 1975). It is true that binaries are, on average, more massive than single stars and would migrate to the core of the cluster, but we have been able to work all the way to the center of M3, so no such selection will suffice to remove them from our sample.

One is led to the conclusion that their current absence reflects an initial absence and that the process of star formation in these systems was probably very different from that currently seen in the solar neighborhood. One should therefore, for example, not approach the problem of the mass function, which we shall presently meet, with any preconceived ideas one might have gleaned from population studies in the Galaxy.

Two other stars, von Zeipel 764 and 911, deserve special attention. They are removed 3.5 and 4.5 standard deviations, respectively, from the cluster mean velocity. There can be little doubt that they are cluster members; both are projected very near the center of the cluster and, on the basis of all reasonable model fits to the cluster, their velocities are less than the escape velocity away from the cluster mean. Neither is of variable velocity; both have been extensively observed. There should be no such stars in a sample of 100, and the probability of two such is less than a part in 10^6. We shall see that these stars must have a special origin, and they will be omitted from the remainder of the analysis. They will be taken up again in Secs. VII and VIII.

III. ASTROPHYSICAL DATA

One cannot, of course, construct a model for the cluster on the basis of velocity data alone. One needs as well data on the distance to the system, the radial distribution of mass (or light), and the mass spectrum of the stars, and, if one relies on the light distribution, some

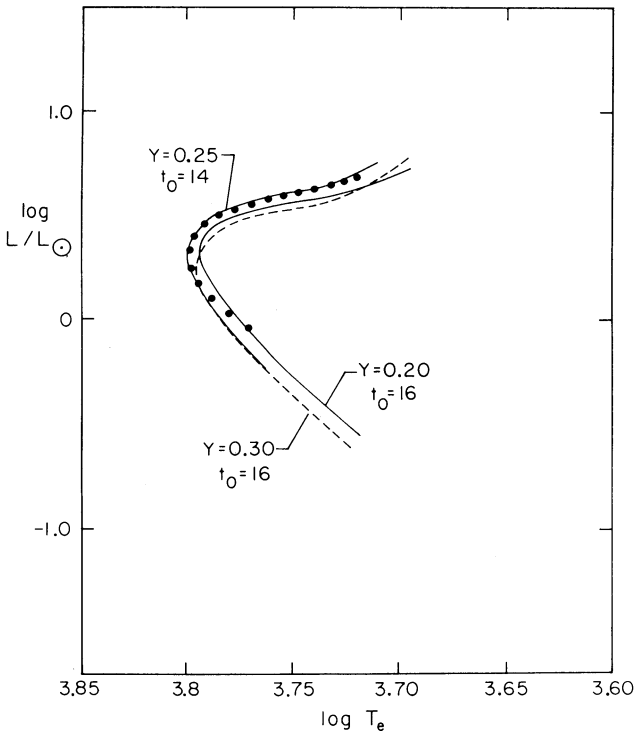

FIG. 1. Theoretical isochrones from Demarque for $Y = 0.2$ (———) and $Y = 0.3$ (···) for $t = 16 \times 10^9$, $z = 0.0004$. The observed locus is also shown for the adopted modulus of 15.08. The fit to a theoretical isochrone interpolated for $Y = 0.25$ and $t = 14 \times 10^9$ yr is quite good.

information about the mass–luminosity relation. We discuss in this section the parameters we have used in fitting the models to the "real" cluster.

a) The Distance Modulus

The distance moduli of the brightest northern clusters have been discussed in detail by Sandage (1970), who obtained a value of 14.83 for M3, as a weighted mean of a number of determinations. The modulus, however, is not really independent of the models chosen for the stars near turnoff, and we have chosen to make a determination which is completely consistent with our mass–luminosity relation, at the risk of some error in the modulus.

Pierre Demarque kindly supplied us prior to publication with detailed isochrones for new population II models near the turnoff for a grid of values of Y, Z, and age (Ciardullo and Demarque 1977). We have compared these models with the photometry of Sandage (1970), transformed to the theoretical $m_{\rm bol}$,logT_e plane by the application of the theoretical colors and bolometric corrections of Böhm-Vitense (1973). In the range of interest, the bolometric corrections are not large. A value of $Z = 0.0004$ is adopted, since that is a value in the Demarque tables, and is near the value (0.0005) suggested as most probable by Sandage (1970). An exhaustive study of M92 and M15 by Böhm-Vitense and Szkody (1973) yielded a helium abundance Y of 0.25 and ages near 14×10^9 yr. The Demarque models have turnoffs that move almost vertically at a given age with Y.

$$\left.\frac{\partial M_{\rm bol,}t_0}{\partial Y}\right|_{t_0} = 2.5 \pm 0.3;$$

$$\left.\frac{\partial \log T_{\rm eff}}{\partial Y}\right|_{t_0} = 0.0 \pm 0.01, \quad (1)$$

and, of course, become bluer and brighter with decreasing age at a given Y,

$$\left.\frac{\partial M_{\rm bol,}t_0}{\partial \log t_0}\right|_{Y} = 2.1 \pm 0.3;$$

$$\left.\frac{\partial \log T_{\rm eff}}{\partial \log t_0}\right|_{Y} = -0.10 \pm 0.020, \quad (2)$$

for $0.2 \lesssim Y \lesssim 0.3$, $t_0 \sim 15 \times 10^9$ yr. The observed cluster HR diagram in the vicinity of the turnoff, transformed into the theoretical plane, is shown with the isochrones from Demarque's model for $Z = 0.0004$, $t = 16 \times 10^9$ yr, and $Y = 0.2$ and 0.3 in Fig. 1. The observed locus is a bit bluer and, if $Y = 0.25$ is chosen, yields a modulus of 15.08 and an age of 15×10^9 yr; the ranges are from 14.96 to 15.20 for Y between 0.3 and 0.2, and 15.02 to 15.14 for ages between $16 \times$ and 14×10^9 yr, respectively. We adopt 15.08 for the modulus.

The corresponding turnoff mass is $0.79 M_\odot$. The fit to the usually troublesome subgiant branch is superb; that below the turnoff is less good, but the bolometric corrections there are almost certainly bad (we used the Böhm-Vitense *giant* bolometric corrections and colors for want of something better), and the models depend critically on the convection theory, as usual, for determination of the effective temperature. All in all, the fit is quite satisfactory, and the agreement with the work of Böhm-Vitense and Szkody reassuring.

b) The Mass–Luminosity Relation

For the upper main sequence and giants we use the Demarque models and assume for the sake of simplicity that all the evolved stars have the turnoff mass. This ignores possible mass loss in advanced stages, but that is almost certainly too rapid to affect a star's dynamics, and the change in the overall mass-to-light ratio is entirely negligible.

For the lower main sequence, which at this stage is really only of academic interest (since it contributes mass but little light), we used the photometric data of Veeder (1974). First the relationship between $M_{\rm bol}$ and M_K, which is very well defined by Veeder's work, was adopted:

$$M_{\rm bol} = 1.118 M_K + 1.78. \quad (3)$$

TABLE III. The adopted mass-luminosity-color relationship for stars below the turnoff.

log$m$	M_{bol}	M_K	$V-K$ (pop II)	M_V (pop II)
−0.15	5.10	...	...	5.25
−0.20	6.15	...	...	6.40
−0.25	6.90	4.58	2.75	7.33
−0.30	7.60	5.20	3.22	8.42
−0.35	8.10	5.65	3.50	9.15
−0.40	8.50	6.01	3.81	9.82
−0.45	8.90	6.37	3.98	10.35
−0.50	9.30	6.72	4.16	10.88
−0.55	9.60	6.99	4.30	11.29
−0.60	9.85	7.22	4.40	11.62
−0.65	10.10	7.44	4.52	11.96
−0.70	10.35	7.66	4.66	12.32
−0.75	10.60	7.89	4.80	12.69
−0.80	10.85	8.11	4.95	13.06
−0.85	11.10	8.33	5.12	13.45
−0.90	11.35	8.56	5.57	14.13
−0.95	11.60	8.78	5.70	14.48
−1.00	11.85	9.05	6.11	15.16

There appears to be very little scatter in the above relation, and no significant trends with kinematics or color. We then used Veeder's (M_{bol}, $V-K$) diagram to define a blue envelope to the observed scatter diagram, which Veeder suggests (as seems reasonable) represents extreme population II on the basis of kinematic evidence. The bolometric correction is then defined as

$$BC = (M_V - M_K) + M_K - M_{bol}$$
$$= (V-K)_{pop\ II}(M_{bol}) - 0.108\,M_{bol} - 1.59. \quad (4)$$

The mass–M_{bol} relationship was taken from Copeland, Jensen, and Jørgensen (1970). Their $Y = 0.25$, $Z = 0.001$ models (with hydrogen molecule formation) fit the lower end of the Demarque models nicely, and extend to −0.6 in $\log(M/M_\odot)$. Below that the relationship was extended to $0.1M_\odot$ with a straight line with slope $dM_{bol}/d\log M = 5.5$, though at these masses the stars are so faint that for our purposes they do not matter at all. The resulting ($\log m$,M_V) relationship is given with intermediate quantities of interest in Table III for stars below the turnoff.

c) *The Mass Function*

The mass function in M3 is a more difficult question. Sandage (1957) has published counts as a function of V down to $M_V = 6.7$ with our modulus. The resulting mass function is strongly curved in the range over which it is defined, $\log m = -0.12$ to −0.22. Da Costa and Freeman (1976) used the fact that this function levels out at the lower end of the range to argue that it fits smoothly on to a Salpeter mass function $dN = Cm^{-(1+x)}dm$ with $x = 1.35$; the actual slope is closer to $x = 0.7$ at the end. We feel strongly that the extreme curvature so near the turnoff mass is almost certainly incorrect. That the power-law slope should change from ∼1 to ∼6, which is what the data taken at face value imply, in a range of 0.10 in log$m$, which furthermore is just the range currently at the top of the unevolved main sequence, seems highly implausible. Since only a few hundredths of a magnitude error in the location of the counting bin boundaries can change the curvature of order itself, we prefer to consider that Sandage's data determine the *slope* of the mass function, but say nothing about curvature. There is no particular reason to use a power-law mass function, of course, but it is a simple form and the range of masses of interest sufficiently small that the exact form does not matter very much. The situation is illustrated in Fig. 2. The slope determined from the Sandage counts, corrected for mass segregation via the models we discuss later, is about $x = 2$, considerably steeper than the Salpeter function.

The mass function must be cut off at low masses, whether by evaporation or, more likely, by tidal shocks (Ostriker, Spitzer, and Chevalier 1972). The form of the mass function near the cutoff is not well determined, nor is the exact value of the cutoff mass. Some choices we have tried for the cutoff are illustrated in Fig. 2; the results are not strongly dependent on either the cutoff mass or the form of the cutoff, since most of these low-mass stars are at large radii, where they do not affect the observable properties of the cluster very much.

In the models we have constructed, the masses are binned in intervals of 0.15 in log$m$, with a heavy white dwarf/neutron star bin at $1.2M_\odot$. The total light in the bin, including the turnoff stars and giants, is calculated from the Sandage luminosity function, and the light-to-mass ratio using our mass function. If M is the total mass in a bin in log$m$, and the upper and lower limits of the bin masses are m_j and m_{j+1} respectively, then for the mass function $dN = C_0\,(m/m_0)^{-x}\,d\ln m$, the masses in the bins are

$$M_j = \frac{C_0 m_0}{(1-x)\ln 10}\left(\frac{m_j}{m_0}\right)^{1-x}\left[1-\left(\frac{m_{j+1}}{m_j}\right)^{1-x}\right]. \quad (5)$$

In Table IV, the bin masses M_j and the total visual light-to-mass ratios λ_j (solar units) are tabulated for various power-law mass functions with no cutoffs. The normalization (i.e., the value of C_0) is arbitrary. It may be clearly seen that the contribution to the light from mass classes 3–7 never amounts to much more than 10% of the total.

The number of stars that have died is given by

$$N_{dead} = \frac{C_0}{\ln 10}\frac{1}{x}\left[\left(\frac{m_0}{m_L}\right)^x - \left(\frac{m_0}{m_u}\right)^x\right], \quad (6)$$

where m_u and m_L are the upper and lower mass limits of interest, presumably infinity and $m_{T_0} = 0.79M_\odot$, respectively, in the present case. The number of white dwarfs is given by this expression with $m_u = m_{WD}$, the mass above which stars do something more exotic than shed their envelopes and become prosaic white dwarfs—probably between 4 and 6 or so solar masses. Neutron stars, if any, come from a somewhat higher range, but one must keep in mind that pulsar data suggest that at least some neutron stars are formed with large velocities, much larger than the cluster escape ve-

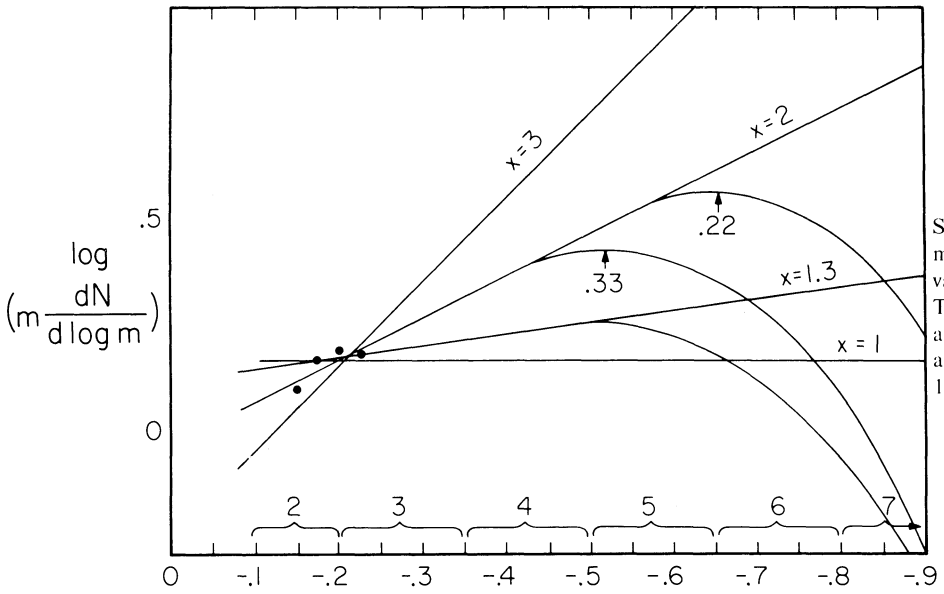

FIG. 2. The segregation-corrected Sandage counts (dots) and various mass function power laws with the various cutoffs used in the models. The mass class bins are indicated along the bottom axis. There is in addition a "heavy remnant" bin at $1.2M_\odot$, mass class 1.

locity, so there may well be none left in the cluster. We will not speculate about higher mass stars yet, but we will be able to place interesting limits on the total mass in heavy remnants. We have assumed that white dwarfs are formed from stars with mass $M = 5M_\odot$ downwards (the number is very insensitive to this upper limit) and have generally assumed that they are distributed equally in total mass among mass classes 1 ($1.2M_\odot$) and 2–4, from which one readily calculates their contribution to M_j. We assume, of course, that they contribute no appreciable light. Neutron stars, if they are included, go into mass class 1.

d) The Surface Brightness Distribution

The run of surface brightness with radius, extended by the use of star counts, is taken from the composite data compiled by Da Costa and Freeman (1976). The treatment of star counts on the same basis as surface brightness is justified, since the counts refer to stars at and above turnoff, and essentially all the light comes from these stars also. We are now ready to discuss the models.

IV. THE MODELS

In lieu of a complete evolutionary treatment of the cluster structure, we have chosen to build models with plausible forms for the distribution function, satisfying the constraints imposed by relaxation processes near the cluster center. King (1965) showed that a "lowered Maxwellian" energy dependence was a good approximation to the solution of the Fokker–Planck equation describing the phase-space diffusion and evaporation of stars from such a system as this one. Possible anisotropies are most easily incorporated in the Mitchie (1963) fashion by a term of the form $\exp(-\beta J^2)$ in the distribution function. We therefore take, for mass class j,

$$f_j(E,J) = e^{-\beta J^2}(e^{-A_j E} - 1), \quad (7)$$

where the zero of energy has been taken to be the energy of a particle at rest at the cluster edge, assumed as usual to be determined by a tidal cutoff, so that stars of positive energy are lost to the system. The short relaxation times in the cluster center demand thermal equilibrium there, so that $A_j \propto \bar{m}_j$, the mean mass of the jth mass class. If ψ is the potential, we can write (7) as

$$f_j(E,J) = \exp(-\beta m_j v_\perp^2 r^2/2r_t^2) \times \{\exp[-\beta(\tfrac{1}{2}m_j v^2 + m_j\psi)] - 1\}, \quad (8)$$

TABLE IV. Bin masses and light-to-mass ratios for various power-low mass functions (no cutoffs).

Bin j	Mass range (log$m$)	Average mass ($M_\odot$)	Light-to-mass ratio ($L_{\odot V}/M_\odot$)	M_j $x = 1$	$x = 1.3$	$x = 1.6$	$x = 2.0$	$x = 2.5$	$x = 3$
2	−0.05, −0.2*	0.72*	6.33	0.937	0.905	0.875	0.838	0.795	0.723
3	−0.2, −0.35	0.53	0.376	1.44	1.52	1.60	1.72	1.89	2.07
4	−0.35, −0.5	0.38	0.038	1.44	1.69	1.97	2.43	3.17	4.16
5	−0.5, −0.65	0.27	0.011	1.44	1.87	2.42	3.43	5.32	8.23
6	−0.65, −0.8	0.19	0.007	1.44	2.07	2.98	4.85	8.93	16.40
7	−0.8, −0.95	0.13	0.003	1.44	2.29	3.67	6.86	15.0	32.8

* The average mass reflects the fact that the maximum mass is 0.79 $M_\odot$, the giant mass, rather than the bin boundary.

where r_t is the anisotropy radius (assumed the same for all mass classes; see the discussion in Sec. VII).

If we adopt a characteristic velocity variance v_0^2 and a characteristic radius r_c and let $W = -\psi/v_0^2$, $\xi = r/r_c$, the Poisson equation becomes

$$\frac{1}{\xi^2}\frac{d}{d\xi}\left(\xi^2\frac{dW}{d\xi}\right) = -4\pi G\rho r_c^2 v_0^{-2}. \quad (9)$$

If we now *define* r_c by the requirement that

$$\rho = \rho_0[1 - \tfrac{3}{2}r^2/r_c^2 + O(r^4)], \quad (10)$$

so that the *projected* mass density has half-power radius r_c, then we obtain (King 1966)

$$4\pi G\rho_0 r_c^2 v_0^{-2} = 9 \quad (11)$$

and

$$\frac{1}{\xi^2}\frac{d}{d\xi}\left(\xi^2\frac{dW}{d\xi}\right) = -9\sigma, \quad (12)$$

where $\sigma = \rho/\rho_0$. All this so far is identical to King's (1966) treatment for single-component models. The run of density for each mass class is given near the center by (we assume at the center that $e^{A_j E}$ is large compared to unity for this discussion)

$$\rho_j = \rho_{j0}\, e^{-\beta m_j(\psi-\psi_0)} \simeq \rho_{j0}\,[1 - \beta m_j(\psi - \psi_0)], \quad (13)$$

and so

$$\rho = \rho_0 - \beta(\psi - \psi_0)\sum_j \rho_{jo} m_j = \rho_0[1 - \beta\bar{m}(\psi - \psi_0)], \quad (14)$$

with the mean mass $\bar{m}$ defined as required, i.e., as a central density-weighted mean

$$\bar{m} = \rho_0^{-1}\sum_j \rho_{0j}\, m_i. \quad (15)$$

Comparison with (10) and (11) requires that $\beta\bar{m}v_0^2 = 1$, which is natural enough, and letting r_{cj} be the core radius of mass class j, we have

$$r_{cj}^2 = r_c^2\,(\bar{m}/m_j). \quad (16)$$

The characteristic velocity v_0 is just the one-dimensional velocity dispersion of a particle of mass $\bar{m}$ in thermal equilibrium in the cluster center. We let $\alpha_j = \rho_{0j}/\rho_0$ be the fractional density contribution of mass class j at the center of the cluster, $\sigma_j = \rho_j/\rho_0$, and $\mu_j = m_j/\bar{m}$.

If we now introduce the dimensionless velocity $u = v/v_0$, we can pose the problem in a completely dimensionless form. The distribution function is

$$\hat{f}_j(\xi,u) = \alpha_j C_j \exp(-\tfrac{1}{2}\mu_j u_\perp^2 \xi^2 \xi_t^{-2}) \times [\exp(-\tfrac{1}{2}\mu_j u^2 + \mu_j W) - 1], \quad (17)$$

where

$$\int_{|u|<(2W)^{1/2}} \hat{f}_j(\xi,u)\,d^3u = \sigma_j(\xi)$$

requires that

$$C_j = \left\{\int_{|u|<(2W_0)^{1/2}} [\exp(-\tfrac{1}{2}\mu_j u^2 + \mu_j W_0) - 1]\,d^3u\right\}^{-1}. \quad (18)$$

It is clear that the densities σ_j can be written

$$\sigma_j(\xi) = \alpha_j \mathcal{I}_1(\mu_j W, \xi/\xi_t)/\mathcal{I}_1(\mu_j W_0, 0), \quad (19)$$

where

$$\mathcal{I}_1(x,y) = \int_{|u|<(2x)^{1/2}} \exp(-\tfrac{1}{2}y^2 u_\perp^2) \times [\exp(-\tfrac{1}{2}u^2 + x) - 1]\,d^3u. \quad (20)$$

The integral (20) can be done numerically once and for all, and tabulated as a function of x and y.

The radial and tangential velocity dispersions can similarly be obtained:

$$\langle u_\xi^2\rangle_j = \mu_j^{-1}\mathcal{I}_2(\mu_j W, \xi/\xi_t)/\mathcal{I}_1(\mu_j W, \xi/\xi_t),$$
$$\langle u_\perp^2\rangle_j = \mu_j^{-1}\mathcal{I}_3(\mu_j W, \xi/\xi_t)/\mathcal{I}_1(\mu_j W, \xi/\xi_t), \quad (21a)$$

where $\mathcal{I}_2$ and $\mathcal{I}_3$ are the appropriate velocity moments, in analogy to Eq. (20). These functions can likewise be tabulated.

The problem then reduces to the solution of the simple ordinary differential equation (12). With W_0, ξ_t, and α_j specified, one integrates (12) until W reaches 0, at which time one has reached the cluster edge. It is most convenient to solve (12) as a first-order *system,*

$$\xi^2\frac{dW}{d\xi} = -U, \quad \frac{1}{\xi^2}\frac{dU}{d\xi} = +9\sigma(\xi, W); \quad (21b)$$

the quantity U is related to the mass contained within radius ξ by (King 1965)

$$M(\xi) = (r_c v_0^2/G)U. \quad (22)$$

Note that U is not the dimensionless mass, but is $9/4\pi$ times it, i.e.,

$$U = 9\int_0^\xi \sigma\xi'^2 d\xi'. \quad (23)$$

There is, of course, mass segregation in these models, so a given mass function for the cluster does not translate in any simple way to the specification of the α_j. This problem is simply solved by iteration. The α_j are first evaluated supposing there is no mass segregation, so $\alpha_j \propto M_j$ for the proposed mass function. They are then multiplied at each step by the ratio of the desired mass function in mass class j to that obtained in the last iteration. In practice, each U_j is kept as the structure equations (21b) are integrated; so one does not have to do any additional work to evaluate the mass functions.

A projection of the cluster model on the sky is then performed, and the line-of-sight velocity dispersion at each point is evaluated.

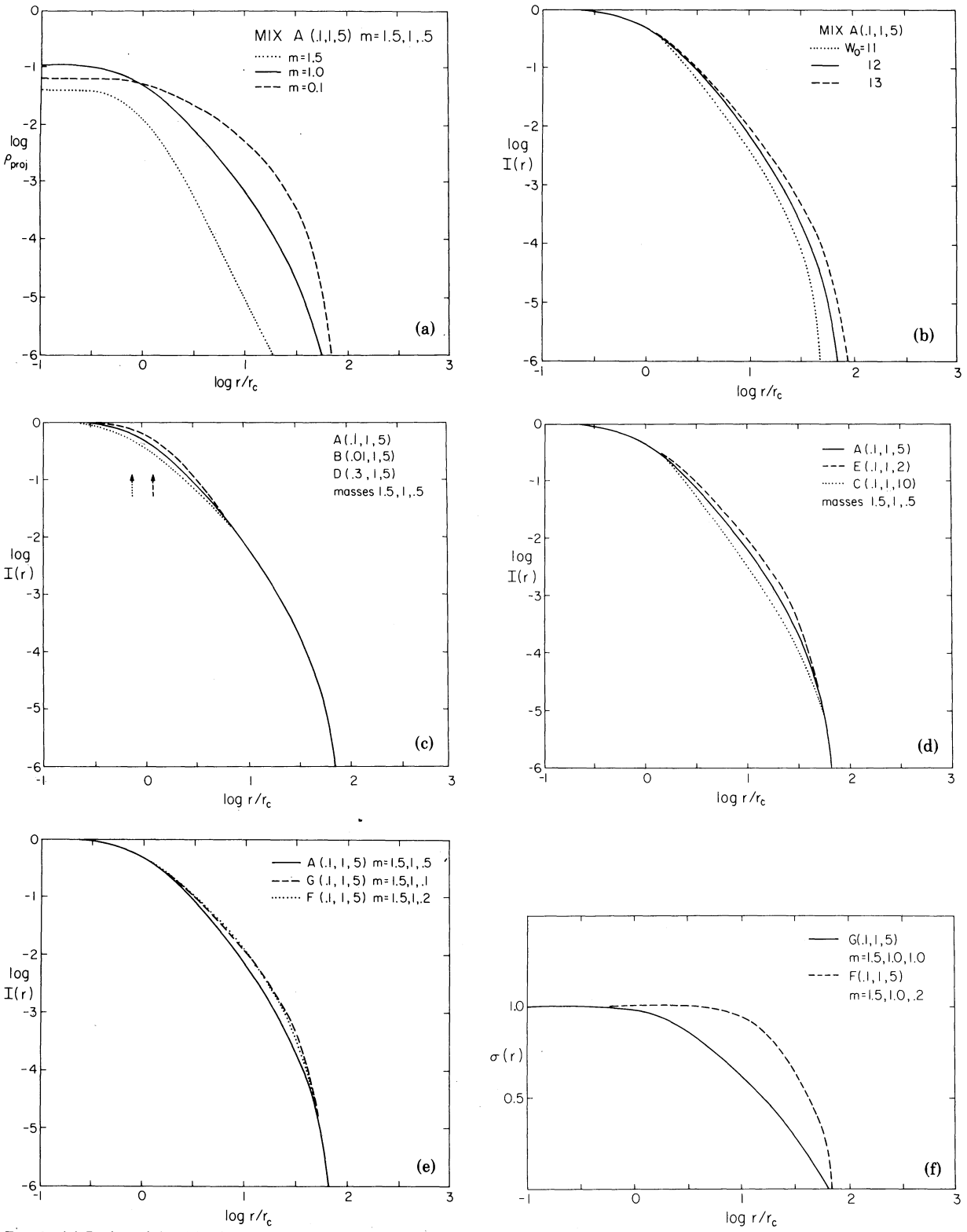

FIG. 3. (a) Projected densities for mass classes 1 (m = 1.5), 2 (m = 1.0), and 3 (m = 0.5) for the three-component isotropic model A, which best fits the light distribution of M3. (b) Projected surface brightness for model A with three values of the central potential W_0. W_0 = 12 is the best-fit model. (c) The dependence of the projected core brightness on the heavy mass fraction M_1. The numbers in parentheses following the model name are (M_1, M_2, M_3). The arrows indicate the scale core radii for the extreme models. (d) The dependence of the projected envelope brightness on the light mass fraction M_3. (e) The dependence of the projected envelope brightness on the mass of the light particles m_3 (see text for discussion). (f) Radial velocity dispersion as functions of radius for the two extreme models in (e).

$$\langle u_{\rm los}^2 \rangle = \int \sigma(\eta)\left(\frac{\zeta}{\eta}\langle u_\xi^2\rangle + \frac{\xi}{2\eta}\langle u_\perp^2\rangle\right)d\zeta,$$
$$\eta = (\xi^2 + \zeta^2)^{1/2}. \quad (24)$$

The projected densities σ_j are multiplied by the light-to-mass ratio λ_j (as amended by the addition of dark remnants) and added to produce the run of surface brightness. Fitting this to the data clearly yields r_c (provided a modulus is known) and the total luminosity of the cluster. The radial velocity data can in principle be fitted to the run of $\langle u_{\rm los}^2 \rangle$ to yield v_0, and the model is completely specified; one obtains masses, densities, radii, etc, by appeal to the relevant scaling equations, all of which depend only on v_0^2, r_c, and dimensionless model parameters.

V. PHENOMENOLOGY: THE THREE-COMPONENT APPROXIMATION

With the scanty data available on the mass function and the complete lack of knowledge about the upper part of the mass function and hence on the remnants to be expected, there is quite a large number of parameters available. To acquire some feeling for what the really relevant ones are and how they interact, we constructed a series of three-component models, and it is perhaps worthwhile to discuss these results in some detail.

Although we shall, in the end, fit the cluster with a seven-component model, it seemed that most of the physics should be contained in models with three, which are (1) Heavy dark remnants, mass m_1, total mass M_1; (2) Giants and turnoff stars, mass $m_2 = 1$, total mass $M_2 = 1$; and (3) Low mass dwarfs, taken to be nonluminous, mass m_3, total mass M_3. Six dimensionless parameters describe these models: m_1, M_1, m_3, M_3, ξ_t, and W_0. A reasonable fit to the light distribution of M3 except in the very outer parts is given by a model with mass parameters roughly appropriate to an $x=2$ mass function cutoff at about $0.3M_\odot$. This model, which we will call model A, has parameters

$$\text{A: } m_1 = 1.5,\ m_3 = 0.5,\ M_1 = 0.1,$$
$$M_3 = 5,\ W_0 = 12,\ \xi_t = \infty.$$

We consider variations about this model.

The radial projected density profiles of the three components are shown in Fig. 3(a). As expected, the heavies, owing to their lower equilibrium velocity dispersion, are much more centrally concentrated than the lighter stars. It is easy to show that in the region away from the core in a roughly isothermal structure, a minor component (one whose density is small compared to the total) with mass m and velocity dispersion $\langle v^2 \rangle$ has a power-law density distribution $\rho \propto r^{-\alpha}$, where

$$\alpha = 2\langle \overline{v^2} \rangle / \langle v^2 \rangle = 2m/\overline{m}, \quad (25)$$

$\langle \overline{v^2} \rangle$ is the velocity dispersion of the dominant component, and $\overline{m}$ its mass. For truncated isothermals such as these cluster models, the slope of the dominant component need no longer be near 2, but the ratio of the slopes is still roughly the ratio of the masses. The slope itself and the outer radius is sensitive to the depth of the central potential, as is shown in Fig. 3(b), where the projected light distribution (projected density distribution for component 2) is shown as a function of W_0 for fixed core radius.

Since the heavy component is so centrally condensed, one would expect that changes in its properties would mostly affect the core shape. The result of varying M_1 with the rest of the parameters fixed except for W_0, which is chosen to give identical envelope profiles, is shown in Fig. 3(c). Notice that it is not simply the core radius which is changed, but the form of the distribution at small radii; for large M_1, the core grows a region of quite shallow slope before it goes over into the envelope. This feature is a sensitive indicator for the presence of heavy remnants and can easily be understood by appeal to Eq. (25). If the heavies dominate the density, the lighter giants are forced to a smaller logarithmic gradient; the more dominant are the heavies, the larger is the radius of this region.

If one varies the mass fraction of the light stars, M_3, one expects the slope of the envelope to change, since the mean mass changes with the proportion of light stars. This is illustrated in Fig. 3(d), where model A and two models with $M_3 = 2$ and 10 are shown, with W_0 adjusted to give the same cluster radius. The variation is as expected; larger M_3 makes a steeper falloff in the light distribution.

There are, however, some surprises. If one varies not M_3 but m_3, the mass of the light component, one would expect the same sort of variation as with M_3; lighter dwarfs should result in a steeper giant distribution, since the mean mass must decrease. Figure 3(e) shows model A with two models for which $M_3 = 5$ but $m_3 = 0.2$ and 1.0, again with W_0 adjusted so that the radii are the same. The two models are different from model A but almost identical to each other! The reason is that, for such light particles, the light component's central concentration is so small that it does not dominate the density until the effects of the energy cutoff are already very strong, and at intermediate radii the middle component dominates. Thus one must be rather careful. The lesson for real cluster models is that the lower mass cutoff, *if it is low enough, has no significant effect on the cluster structure* as traced by the giants. The only effect of extending it to quite low masses is to dump a large amount of mass at very large radii.

So far we have not looked at dynamical information at all. If we consider the run of projected velocity dispersion in component 2 with radius, these two models are quite different, as shown in Fig. 3(f): The giant velocity dispersion holds up much longer in the model with very light stars, so they can be distinguished if one has radial velocities. For comparison, Fig. 4(a) shows the projected velocity dispersion curves for models with the population

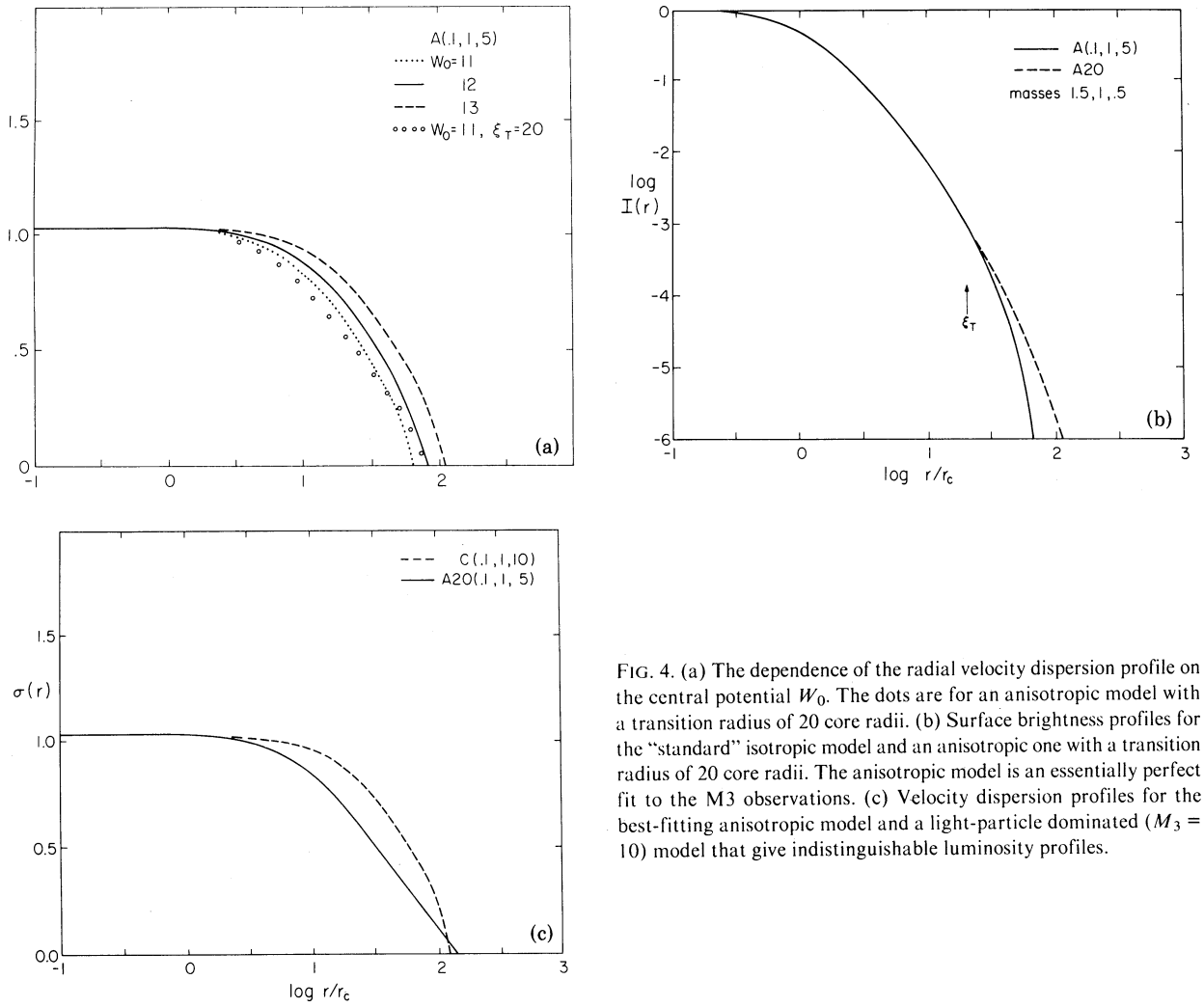

FIG. 4. (a) The dependence of the radial velocity dispersion profile on the central potential W_0. The dots are for an anisotropic model with a transition radius of 20 core radii. (b) Surface brightness profiles for the "standard" isotropic model and an anisotropic one with a transition radius of 20 core radii. The anisotropic model is an essentially perfect fit to the M3 observations. (c) Velocity dispersion profiles for the best-fitting anisotropic model and a light-particle dominated (M_3 = 10) model that give indistinguishable luminosity profiles.

parameters of model A, but with different W_0's; here the curves do not change *shape* but simply move to larger radii as one increases W_0, thus flattening the density distribution.

All the above models are isotropic; $\xi_t = \infty$. The effect of anisotropy in these models is quite different from that in single-component ones. There there ensues a steep increase in logarithmic slope of the density with radius at ξ_t, which flattens out again after an increase of a factor of 5 or so in radius, provided the system radius is large enough. This decrease is brought about by the decrease in the velocity integral over the distribution function corresponding to the smaller width in the tangential velocity distribution for $\xi \gtrsim \xi_t$. Eventually the potential feels the strong decrease in density, and the system then settles to the isothermal with purely radial orbits, for which $\rho \sim r^{-2}(\ln r)^{-1}$. In the multicomponent systems, the dominant component (for models of interest, component 3) behaves this way, but the giants respond primarily to the decreased rate of growth of the potential, and actually fall off more *slowly* than they do in the isotropic models. Figure 4(b) shows model A and one with an identical population (W_0 is adjusted to give the same profile interior to ξ_t) with ξ_t = 20, called here A20.

This model has been chosen to be an excellent representation to M3 over the whole observed range of radius. There is, however, an isotropic model with an almost identical light distribution, one with a population considered above: m_i = (1.5, 1.0, 0.5), M_i = (0.1, 1, 10) —i.e., a very light-star-dominated model. The light distribution is so nearly identical with that shown for A20 that the difference cannot be seen on the scale of the figures. Again dynamics can come to the rescue, as seen in Fig. 4(c), where the velocity dispersions are shown for these models. The anisotropic one has a projected velocity dispersion which falls off much more rapidly with radius. The total mass-to-light ratios are also very different, of course, though the values for *core* mass-to-light are almost identical, since neither the light star population nor the anisotropy makes itself felt there. We shall see that there are difficulties fitting the observed cluster

with isotropic models that satisfy the dynamical constraints imposed by our velocities.

We have found the three-component models of great help in developing intuition about what the various parameters at our disposal do, and they have lent credence (at least in our minds) to the hope that our model fits to M3 are not too far from reality.

VI. THE FITTING PROCEDURE

From the observed light distribution and our sample of radial velocities, we must find a "best" fit to a model. We have chosen to give the fit to the light precedence, since the data are of much higher precision. (The velocity *dispersion,* which one fits, is of necessity highly stochastic in nature, and from the measurements of about 110 velocities, even with infinite precision, has of necessity $\sim 7\%$ overall error, much higher as soon as one attempts to extract any detail from it.) Fitting the dispersion is not easy, nor is assessing the goodness of fit.

The first parameter we determine is the core radius r_c. To do this, we want to fit the core of the projected model to the core of the cluster, but do not want to be too sensitive to small deviations in the core shape between the model and the cluster. The question is clearly how to weight the least-squares fit, and we arrived, after some experimentation, at a scheme which minimizes

$$\epsilon = \sum_{\text{rings}} \frac{1}{B_j} [L\tilde{I}(\gamma_j/\gamma_c) - B_j]^2, \tag{26}$$

where B_j is the observed surface brightness, in ring j γ_c is the angular core radius, $\tilde{I}(\xi)$ the projected model surface brightness, γ_j the angular radius corresponding to B_j, and L an overall scale factor connecting model and real surface brightnesses. L and γ_c are varied to minimize ϵ. In fact the analysis is not carried further unless the fit to the surface brightness distribution is quite good. The parameters which one has at one's disposal to improve the fit are the mass function slope, which is analogous to the quantity M_3 in the three-component models, the anisotropy, and the mass in heavy remnants, analogous to M_1, to get the core shape right. The heavy remnant mass also has a very large effect on the core M/L ratio, since stars of large mass have small core radii and steep density falloffs.

Given a fit to the surface brightness, we now want to determine the velocity scale v_0, taking into account the "jitter" discussed in Sec. I and the measuring errors. To do this, we assume that the projected velocity distribution at each radius is Gaussian, which is a good approximation, and that the distribution of errors is also Gaussian, which seems also to be a good approximation. Thus the observed velocity of star j is

$$v_{\text{obs},j} = w_j + \bar{v} + \epsilon_j, \tag{27}$$

where w_j is the real projected random velocity of star j, $\bar{v}$ is the systemic velocity of the cluster, and ϵ_j is the error, compounded of the jitter and the measuring error, for which $\langle \epsilon_j \rangle = 0$ and $\langle \epsilon_j^2 \rangle^{1/2} = \Delta_j$. Dropping the subscript "obs" for brevity, the probability density function for v_j is, if a given model describes the real velocity distribution,

$$P_j = P(v_j) = [2\pi(v_0^2\eta_j^2 + \Delta_j^2)]^{-1/2} \times \exp[-(v_j - \bar{v})^2/2(v_0^2\eta_j^2 + \Delta_j^2)], \tag{28}$$

where v_0 is the desired velocity scale, and η_j is the projected dimensionless velocity dispersion in the model at the radius ξ_j corresponding to the star's angular radius γ_j. The likelihood function $\mathcal{L}$ is then given by

$$\ln\mathcal{L} = \sum_j \ln P_j = \sum_j \left[\frac{-(v_j - \bar{v})^2}{2(v_0^2\eta_j^2 + \Delta_j^2)} - \tfrac{1}{2}\ln(v_0^2\eta_j^2 + \Delta_j^2)\right]. \tag{29}$$

The maximum-likelihood estimator for v_0 is then given by the solution to $\partial\mathcal{L}/\partial v_0 = 0$, and for $\bar{v}$ by $\partial\mathcal{L}/\partial\bar{v} = 0$; the resulting equations are

$$\sum_j \left[\frac{-(v_j - \bar{v})^2\eta_j^2}{(v_0^2\eta_j^2 + \Delta_j^2)^2} - \frac{\eta_j^2}{v_0^2\eta_j^2 + \Delta_j^2}\right] = 0, \tag{30}$$

$$\bar{v}\sum_j (v_0^2\eta_j^2 + \Delta_j^2)^{-1} = \sum_j v_j(v_0^2\eta_j^2 + \Delta_j^2)^{-1}. \tag{31}$$

If, as is the case with our data, the errors Δ_j are small compared to the cluster dispersion $v_0\eta_j$, the equations can be solved easily by iteration.

Suitable tests for goodness of fit have been somewhat elusive; powerful tests for estimators of variance seem to be lacking in the statistical repertoire. The task seems easy enough. The quantities

$$x_j = (v_j - \bar{v})/(v_0^2\,\eta_j^2 + \Delta_j^2)^{1/2} \tag{32}$$

should be approximately normally distributed with zero mean and unit standard deviation. The difficulty comes because standard tests for the homogeneity of variance [the classical F test, Bartlett's test, etc.—see Burr (1974) for a discussion] all depend on binning the data, and the outcome depends on binning in a way which makes it difficult to say *a priori* how they should be binned. What we need, and so far lack, is a test which looks for significant *trends* (with radius, say) in the unbinned data. The nearest we have been able to come is a test which the authors believe is original, which makes use of the fact that the sum of the squares of two independent, univariate, normal stochastic variables has a chi-squared distribution with one degree of freedom, which in turn is a simple exponential. Since the interval between events in a Poisson process (like shot noise, say) is also exponential, the following cumulative test is suggested.

Order the stars by projected radius, and let

$$Y_j = x_{2j-1}^2 + x_{2j}^2; \tag{33}$$

the distribution function is, if $\langle x_j \rangle = 0$, $\langle x_j^2 \rangle = 1$, and x_j is normal,

$$P(y)dy = e^{-y}dy. \tag{34}$$

Let $Y_k = \sum_{j=1}^{k} y_j$ be the coordinate of the kth event. This set of points on the line is evidently the realization of a Poisson stochastic process, since the y_j are independent and their interval has the exponential distribution (34). Thus the number of "events" in any interval is distributed in a Poisson fashion with mean and variance both given by the length of the interval.

If the η_j do not accurately describe the model, the Poisson nature of the distribution is not disturbed, but the Poisson frequency now changes along the Y axis. The necessity of binning is still present, but the data are now by their nature more or less uniformly distributed, and the dependence on the bin boundaries almost disappears. It becomes now easy by means of any of a wide variety of standard, powerful tests on the *mean* to test for the homogeneity of the distribution.

Before we discuss the fits to M3, let us digress for a bit and consider some effects of two-body relaxation processes that are relevant to the discussion of the cluster structure.

VII. RELAXATION PHENOMENA

Spitzer (1969) gives an expression for the thermal relaxation of two intermixed populations of charged particles, a "field" population whose density is ρ_f, mass m_f, and mean square velocity $\langle v_f^2 \rangle = 3/2l_f^2$, and a "test" population with ρ, m, and l. For our case (gravitation instead of electrostatic forces), the expression becomes

$$1/t_{\rm eq} = {}^{8}\!/_{3}\,(2\pi)^{1/2}\, m\rho_f G^2 \times \ln\Lambda[2^{3/2}\,(1/l^2 + 1/l_f^2)^{-3/2}]. \quad (35)$$

The logarithm term is roughly $\ln(v_0^2 R/G\overline{m})$, where R is some characteristic radius for the system and has a value near 13 for the parameters relevant to our models. Using Eq. (11) and the definition of the dimensionless density σ_j, and the fact that the rates for a given mass class j must be the sum of the rates considering all mass classes as the "field" population (including the test population), we obtain

$$\mathcal{R}_j(\xi) = \frac{1}{t_{{\rm eq},j}} = 18\left(\frac{6}{\pi}\right)^{1/2}\left[\frac{G(m_j/\mu_j)}{r_c^2 v_0}\right] \times \ln\Lambda\left[\mu_j \sum_k \sigma_k(\xi)(\langle u_k^2\rangle + \langle u_j^2\rangle)^{-3/2}\right]. \quad (36)$$

The average rate for mass class j is clearly the density-weighted average of $\mathcal{R}_j$ over the cluster:

$$\overline{\mathcal{R}}_j = \frac{1}{t_{{\rm eq},j}} = 18\left(\frac{6}{\pi}\right)^{1/2}\left[\frac{G(m_j/\mu_j)\ln\Lambda}{r_c^2 v_0}\right]\mu_j \times \int \sigma_j\sigma_k(\langle u_k^2\rangle + \langle u_j^2\rangle)^{-3/2}\xi^2 d\xi \Big/ \int \sigma_j \xi^2 d\xi. \quad (37)$$

Clearly the ratio m/μ is independent of mass class and is just the scale of the dimensionless particle masses; this dimensionless parameter has not entered before because it is irrelevant to the cluster structure. The relaxation rate in the cluster center can be written

$$\mathcal{R}_j(0) = (3/\pi^{1/2})[G(m/\mu)\ln\Lambda/r_c^2 v_0] \times \left[2^{3/2}\mu_j \sum_k \alpha_k \left(\frac{1}{\mu_j} + \frac{1}{\mu_k}\right)^{-3/2}\right] \equiv \mathcal{R}_0\left[2^{3/2}\mu_j \sum_k \alpha_k \left(\frac{1}{\mu_j} + \frac{1}{\mu_k}\right)^{-3/2}\right]. \quad (38)$$

Note that the thermal relaxation time defined here is about 10% shorter than the usually defined energy exchange time.

In considering the decay of anisotropy, another closely related time is of relevance. The *deflection* time $t_{d,j}$ is

$$1/t_{d,j} \simeq {}^{2}\!/_{3}3^{3/2}(8\pi G^2 m_f \rho_f \ln\Lambda) \times l_j^3\,(1 - e^{-1.2l_f/l_j}), \quad (39)$$

where we have taken the mean velocity of a particle in class j, $(3/2l_j^2)^{1/2}$, as representative of the thermal average, and used a crude (~10%) approximation to the function $[\Phi(x) - G(x)]$ that is relevant to this process (Spitzer 1962). In terms of the model parameters,

$$1/t_{d,j} = \mathcal{R}_d\langle u_j^2\rangle^{-3/2} \times \sum_k \mu_k\sigma_k(1 - e^{-1.2\langle u_j^2\rangle/\langle u_k^2\rangle}) \quad (40)$$

at a given radius ξ, where $\mathcal{R}_d = 9\pi^{1/2}\mathcal{R}_0 \simeq 16.0\mathcal{R}_0$.

It is clear, upon reflection, that the decay of anisotropy near the anisotropy radius ξ_t is determined essentially by the *local* value of $t_{0,j}$ even though a typical particle in the cluster models has an orbit which carries it over the better part of a decade in radius. This is basically because for $\xi < \xi_t$ the distribution is isotropic and scattering can only remove and replace particles from a given orbit with equal rates, and far outside ξ_t the scattering is negligibly small compared to its value at ξ_t, on account of the steep falloff in σ. It is also worth noting that for the anisotropy radii of interest, $\xi_t \gtrsim 10$, the expected differences in $t_{0,j}$ from one mass group to another are not as large as might be suspected. At the cluster center, $\langle u_j^2\rangle^{-3/2} \propto m_j^{3/2}$, but the velocity dispersion of the low-mass mass classes drops off much more rapidly with radius than that of the high-mass ones. In the best-fitting M3 models, the total range in velocity dispersion is only a factor of about 1.3 at the inferred anisotropy radius ($\xi_t \sim 15$), which results in a somewhat smaller factor in radius for a given t_d. Thus, if the anisotropy radius is determined by relaxation, the assumption of a fixed ξ_t for all mass classes must be approximately correct.

The run of t_d with radius for the "best" M3 model (model 8; see Sec. VIII*a*) for several mass classes is shown in Fig. 5. The unit of time is the central deflection time $\mathcal{R}_d^{-1}$, 9.5×10^6 yr for this model.

If the anisotropy radius is determined by the initial conditions through the initial violent relaxation, or later through tidal shocks or any other large-scale gravitational perturbations, one would expect no dependence on mass. One exception, which tends to make the *light*

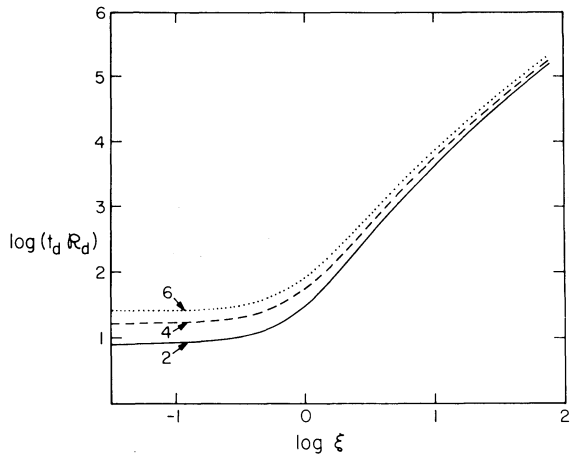

FIG. 5. The deflection relaxation times in units of $\mathcal{R}_d^{-1}$ (9.5×10^6 yr for the model) for model 8 (see table V) for mass classes 2 ($0.720M_\odot$, solid line), 4 ($0.380M_\odot$, dashed line), and 6 ($0.190M_\odot$, dotted line).

particles more nearly isotropic than the heavy ones, is that, since the light particles are much less centrally condensed, they are, as is well known, easier to remove by tidal forces. The population of light particles at large radii, however, is largely supplied by orbits that are quite elongated, and the preferential evaporation of these stars makes the distribution at smaller radii more nearly isotropic. Since the heavies are hardly affected by evaporation, the effect is much less pronounced for them. In any case, it would seem that one should not expect large variations in ξ_t with j.

The consideration of the last relaxation phenomenon we wish to discuss is motivated by the existence of the two "interlopers," the very-high-energy stars that we remarked in Sec. 1 should not be there on statistical grounds. "Should not" statistically is one thing; "should not" physically is another. Stars so far out in the wings of the velocity distribution are acted upon by dynamical friction, and one may well ask whether orbits such as these can possibly have lasted the suggested age of the cluster. If so, they could be artifacts of the initial conditions. If not, they must have been produced by dynamical processes in the cluster since its formation. We comment on this point later.

For stars moving at several times the rms velocity, the frictional slowing-down rate is given by (Spitzer 1962)

$$\frac{1}{t_s} = \left(\frac{1}{v}\frac{dv}{dt}\right) \simeq \frac{(1+m/m_f)4\pi G^2 m_f \rho_f \ln\Lambda}{v^3}, \quad (41)$$

or

$$\frac{1}{t_{s,j}} = \frac{9}{u^3}\left[\frac{G(m/\mu)}{r_c^2 v_0}\right]\ln\Lambda \sum_k (\mu_j+\mu_k)\sigma_k$$

$$= \mathcal{R}_s \left(\sum_k (\mu_j + \mu_k)\sigma_k/u^3, \quad (42)\right.$$

where $\mathcal{R}_s = 3\pi^{1/2}\mathcal{R}_0 \simeq 5.32\mathcal{R}_0$.

Now if $\mathcal{E}$ is the dimensionless energy per unit mass (we take $\mathcal{E} = 0$ at $\xi = 0$ with the particle at rest, so that $\mathcal{E} = \frac{1}{2}u^2 - W + W_0$), then

$$\frac{d\mathcal{E}}{dt} = -\mathcal{R}_s \sum_k (\mu + \mu_k)\sigma_k u^{-1}, \quad (43)$$

where $j = 2$, $\mu = \mu_2$ is the case of interest. This expression breaks down for $u \lesssim 1$, since Eq. (41) holds only for $v \gtrsim l_f^{-1}$; in fact, there are net energy *gains* for $u < 1$. We shall in this approximate treatment neglect those processes, since they occur at the apocenter, where the densities are low and the timescales long, and simply cut off the integrals at $u = 1$. Then the loss averaged over an orbit is

$$\frac{d\mathcal{E}}{dt} = -\mathcal{R}_s \int_0^{\xi_1} (\mu+\mu_k)\,\sigma_k u^{-2} d\xi \Big/ \int_0^{\xi_m} u^{-1} d\xi, \quad (44)$$

where we have assumed that the orbit is strictly radial, ξ_1 is the radius at which $u = 1$, and ξ_m is the apocenter radius. The assumption of radial orbits cannot be far wrong, since both stars are seen projected on the core, and their radial velocities will carry them to very large radii.

The average rate of decay $\langle d\mathcal{E}/dt\rangle = -\mathcal{R}_s g(\mathcal{E})$ is now given as a function of $\mathcal{E}$ alone, and the equation

$$\frac{1}{\mathcal{E}}\frac{d\mathcal{E}}{dt} = \frac{2}{u_m}\frac{du_m}{dt} = -\frac{\mathcal{R}_s}{\mathcal{E}} g(\mathcal{E}) \quad (45)$$

can be integrated to yield the evolution of $\mathcal{E}$ with time. The dependence of u_m, the maximum central velocity ($\mathcal{E} = \frac{1}{2}u_m^2$) on time in units of $\mathcal{R}_s^{-1}$ for the "best" M3 model, which we will discuss in detail in Sec. VIII, is plotted against time in units of $\mathcal{R}_s^{-1}$ in Fig. 6. The value of $\mathcal{R}_s^{-1}$ is of order 2×10^7 yr, and it is clear that, in order that the interlopers survived until now, they had to begin with quite large energies; we will discuss details in Sec. VII.

Since the net result of weak-encounter, diffusive processes is to slow such stars down, one must look to rarer events if they are to be produced and not simply be

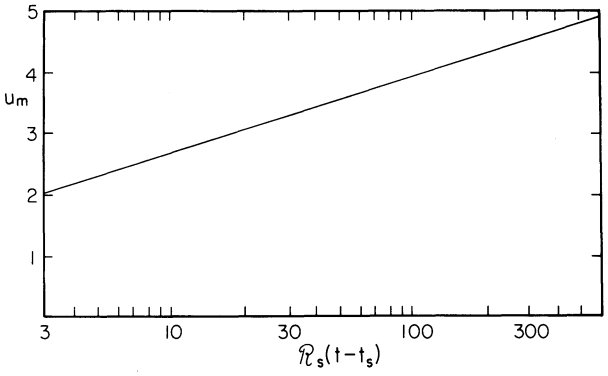

FIG. 6. The frictional decay of high-energy radial orbits in model 8 (see Table V). The quantity m is the maximum orbital velocity; the unit of time $\mathcal{R}_s^{-1}$ in the model is 2×10^7 yr.

leftovers from the beginning. Two processes one can think of are binary disruption and very favorable strong two-body encounters. Binary disruption is almost certainly *not* responsible, since to disrupt a binary system requires the sudden loss of half or more of the system mass, which almost certainly must involve a supernova event in which *more* than half of the primary mass is lost. On current motions of stellar evolution such a star must be of at least about 4 or 5 solar masses, and the evolution time is so short that one may as well be discussing initial conditions. Strong binary encounters are not much better. An optimal collision between two stars of comparable mass can increase the velocity of the faster one by a factor of $\sqrt{2}$ at most, and that in the limit in which both stars are traveling at the same velocity and collide at right angles. Thus the rate of production of stars that we now see as giants traveling at, say, α or more times the one-component rms velocity of that population ($v_0\mu^{-1/2}$), must be roughly

$$r = \int n_g n_f \frac{\Delta\Omega_{\rm in}}{4\pi} v_{\rm rel}\, \sigma \frac{\Delta\Omega_{\rm out}}{4\pi} [P(2^{-1/2}\alpha)]^2 d^3x, \tag{46}$$

where n_g is the present number density of giants (note that we do *not* require the star to have been a giant when it was accelerated), n_f the number of relevant scatterers, $\Delta\Omega_{\rm in}$ the acceptable solid angle of approach, $v_{\rm rel}$ the relative velocity, σ the cross section for scattering through roughly a right angle, $\Delta\Omega_{\rm out}$ the acceptable range of solid angle of egress for the accelerated star, and $P(x)$ the probability of a given star traveling at a speed in excess of x times the rms velocity. We take σ to be half the total strong collision cross section,

$$\sigma \simeq 2\pi G^2 m^2 / v_{\rm rel}^4. \tag{47}$$

The quantity $\Delta\Omega_{\rm in}/4\pi$ is perhaps $\frac{1}{4}$, corresponding to a broad equatorial band. The accelerated star must leave close to the desired "forward" direction, so $\Delta\Omega_{\rm out}/4\pi$ is probably somewhat smaller, say 0.15. Near the core, the energy cutoff is not important, and it is only near the core that the process is likely to occur, if at all; so the function $P(x)$ is

$$P(x) = \left(\frac{2}{\pi}\right)^{1/2} \int_x^\infty y^2 e^{-y^2/2}\, dy \sim \left(\frac{2}{\pi}\right)^{1/2} x\, e^{-x^2/2} \tag{48}$$

for $x \gtrsim 2$. If we take the distribution of density of the giants and scatterers as $\sigma \sim (1+\xi^2)^{-3/2}$, which is not far wrong (the *total* density is more like $(1+\xi^2)^{-1}$, but the giants are heavier than the mean particle mass and hence their distribution steeper), one can do the spatial integral and obtain

$$r \simeq \frac{9N_g}{16\pi \ln(2\xi_e - 1)} \left(\frac{\Delta\Omega_{\rm obs}}{4\pi}\right)\left(\frac{\Delta\Omega_{\rm in}}{4\pi}\right)\left(\frac{\Delta\Omega_{\rm out}}{4\pi}\right) \times \left[\frac{G(m/\mu)t_c}{r_c^3}\right] \frac{\mu^{5/2}}{\alpha} e^{-\alpha^2/2}, \tag{49}$$

where N_g is the total number of giants observed, ξ_e is the radius of the cluster, and $\Delta\Omega_{\rm obs}/4\pi$ is the cone of solid angle pointing nearly enough in the direction of the observer that the star has approximately its total velocity in the line of sight; we take this quantity to be $\frac{1}{4}$ as well, though this is a bit generous. For $N_g \sim 100$, $\xi_e \sim 100$, the leading coefficient is about 4. The product of the solid angle factors is about 10^{-2}. The dimensional factor in square brackets is about 10^{-2} of the central relaxation rate [cf. Eq. (38)]; the $\mu^{5/2}\alpha^{-1}$ factor is typically somewhat less than unity, and $e^{-\alpha^2/2}$ is 10^{-2} for α as small as 3. (Recall that the interlopers had values of α of 3.5 and 4.5.) Thus $r \lesssim 2.5 \times 10^{-6}\mathcal{R}_0$; the corresponding time is in all cases more than 10^{13} yr, and so *no such stars* should have been produced by strong encounters. We shall see that it is not completely implausible that they should have survived from early times.

VIII. THE FIT TO M3

a) Constraints and Models

The fit to the cluster is by no means unique. The statistics of the velocities are not sufficiently good with 107 velocities to distinguish between even fairly extreme possibilities with much significance, but it is possible to delineate "allowed" areas in the parameter space. Other arguments can in some cases be marshaled to support or reject models.

The parameters at our disposal are x, the mass function slope, the low-mass cutoff (here characterized by m_p, the mass at which the mass function peaks (see Fig. 2), and the mass in high-mass remnants. We have chosen to keep the total number of white dwarfs for a given x fixed and consistent with all stars heavier than the current turnoff ($0.79M_\odot$) but less massive than $6M_\odot$ having become white dwarfs; we consider neutron stars and black holes of yet greater mass later.

Our standard assumption for want of something better is that the white dwarfs contribute equal total *masses* to each of mass classes 1 ($1.2M_\odot$), 2 ($0.72M_\odot$), 3 ($0.53M_\odot$), and 4 ($0.38M_\odot$). This yields a mean white dwarf mass of $0.6M_\odot$. We shall vary the fraction in mass class 1, keeping the numbers constant and the contribution to the other mass classes equal. This has the effect, as we have seen, of varying the core shape.

It is important to point out that there is a serious uncertainty concerning the core shape, arising not from observational error but from statistics. The mean luminosity per star in the second mass class, from which all the light in the core (and, indeed, nearly all the cluster) comes, is about $4.2L_\odot$ per star; the mean *square* luminosity is $440(L_\odot)^2$ per star; thus the variance in luminosity per star is about $420(L_\odot)^2$. Thus, if one takes a region with total luminosity $\mathcal{L}$, the variance in $\mathcal{L}$ is of order $100\mathcal{L}$, if $\mathcal{L}$ is in $L_\odot$, and the fractional uncertainty (standard deviation) is $10\mathcal{L}^{-1/2}$. The core of M3 has a projected luminosity of about $3 \times 10^4 L_\odot$, so the associated uncertainty compared to a smooth light distribution,

TABLE V. Properties of the models.

Model	x	ξ_t	Mass in 1.2 $M_\odot$ WD	Mass at peak ($M_\odot$)	$B(r)$ fit and comments	$(M/L)_{mod}$	$(M/L)_{dyn}$	$\sigma(r)$ fit	r_c (pc)	r_{lim} (pc)	V_0 (km/s)	M_{tot} ($10^5 M_\odot$)
1	1.3	∞	all	0.30	none, too convex	...	...	...	...	...	...	...
2	1.3	∞	½	0.30	poor, too convex	...	...	...	...	...	...	...
3	1.3	∞	none	0.30	fair, too convex	1.45	1.92	fair	1.65	103	5.25	5.21
4	2	∞	all	0.33	none, too convex	...	...	...	...	...	...	...
5	2	∞	½	0.33	none, too convex	...	...	...	...	...	...	...
6	2	∞	none	0.33	none, too convex	...	...	...	...	...	...	...
7	2	15	all	0.33	fair, core,[a] extended	2.09	2.00	good	0.93	195	5.67	5.39
8	2	15	½	0.33	good, sl. extended	2.07	2.20	good	1.26	189	4.78	5.96
9	2	15	none	0.33	good	2.06	2.51	good	1.83	191	5.31	6.78
10	2	∞	all	0.23	none, too convex	...	...	...	...	...	...	...
11	2	∞	½	0.23	fair, too convex	2.88	2.70	poor	1.20	113	4.45	7.30
12	2	∞	none	0.23	good	2.86	3.26	poor	1.70	145	5.07	8.82
13	2	30	all	0.23	fair, too convex	2.89	2.36	fair	1.16	106	4.38	6.39
14	2	30	½	0.23	good	2.88	2.66	fair	1.40	124	4.60	7.19
15	2	30	none	0.23	fair, too extended	2.86	3.40	poor	1.70	179	5.10	9.18
16	2	15	all	0.23	fair, too extended	2.89	2.55	good	1.08	226	4.54	6.90
17	2	15	½	0.23	poor, too extended	2.88	...	...	...	...	...	...
18	2	15	none	0.23	none, too extended	2.86	...	...	...	...	...	...
19	3	∞	all	0.30	fair, too convex	3.30	2.89	poor	1.40	121	4.48	7.82
20	3	∞	½	0.30	good	3.23	3.21	poor	1.57	139	4.70	8.68
21	3	∞	none	0.30	fair, too extended	3.22	3.60	poor	1.92	162	5.13	9.72

[a]The fit to the core indicates rather too much dominance by mass class 1.

brought about simply because the core contains a finite number of discrete stars, is about 6%. The uncertainty in the *shape* of the core is substantial. Thus, though we will insist on very good fits to the luminosity distribution through most of the body of the cluster, the core must not be required to fit perfectly.

The fractional uncertainty in the mass-to-light ratio stemming from the finite number of velocity measurements (and this is the largest *statistical* error) is about $(2/N)^{1/2}$, or about 14% (standard deviation). The cutoff in the distribution function should reduce this by a small amount, and the observed dispersion in the squares of the velocities about the mean square is significantly smaller than predicted by a normal distribution. We shall adopt $0.9(2/N)^{1/2}$ as the fractional standard deviation of the square of the velocity dispersion for a group of N stars; the standard deviation of the dispersion itself is, of course, half that.

The situation for the suite of models we have tried is summarized in Table V and in Figures 7 and 8. Table V lists the values of x (1.3, 2, or 3), the anisotropy radius, the mass in $1.2M_\odot$ remnants, the mass at which the mass function peaks, a qualitative description of the fit to the luminosity profile, the *model M/L* (the value calculated from the input stellar population), the *dynamical M/L*

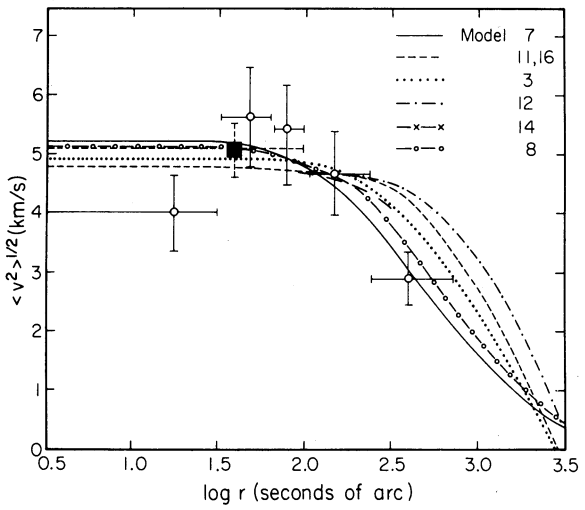

FIG. 7. The observed M3 radial velocity dispersion binned in radius, together with model profiles. Model 8 is the suggested fit. The large black square with the dotted error bars is the average of the first three bins. The horizontal error bars merely indicate the size of the radial bin.

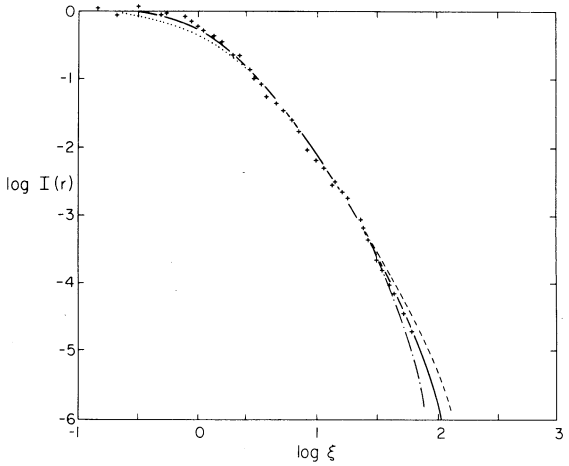

FIG. 8. The fit (model 8) to the observed surface brightness. Portions of three other models are also shown with "fair" fits illustrating the remarks "core" (···), "too convex" (-·-), and "too extended" (– – –).

(the fitted total mass over the total measured luminosity), a qualitative description of the fit to the run of velocity dispersion with projected radius, the core radius r_c and the cutoff radius of the model in parsecs, the velocity scale v_0 in kilometers per second, and the total mass in solar masses. [The meaning of the entries in column 4 is as follows: equal masses in each mass class ("all"), half as much mass in the $1.2M_\odot$ bin as in the other three ("½"), and no $1.2M_\odot$ remnants at all ("none"). The fit to the core shape is already marginal in all cases with "all," so we did not try increasing the fraction.] In each case the central potential W_0 has been adjusted to produce the best fit to $B(r)$, if there is a reasonable fit at all. Figure 7 compares the velocity dispersions of the sample in four radial bins of 21 stars each and an outermost one of 23, with several models that span the range of behavior exhibited. The vertical error bars are 1σ in the dispersion (total length 2σ). The horizontal ones merely indicate the span in radius over which stars contribute; the point is at the mean of the log of the radius for the bin, as is appropriate for this plot. Figure 8 shows the surface brightness profile with model fits illustrating "good," "fair," and "poor" fits.

There is a suggestion (albeit not significant) that the velocity dispersion falls in the core, as might be expected if the core giants were more massive—as they might be as the result of close binary evolution, for example. There is more than a suggestion that the outermost point is low, and furthermore, lower than the prediction of any of the isotropic models. As expected from the three-component models, those models which achieve fits by an extended or dwarf-heavy mass function have velocity dispersions that do not fall off significantly with radius until nearly the limiting radius; models 11, 12 ($x = 2$, peak at 0.23) and 16 ($x = 3$) exhibit this behavior strongly and do not fit the run of velocities at all well, though their mass-to-light ratios are acceptable. Model 3 is essentially the model of Da Costa and Freeman (1976), which fits the velocities acceptably, though not well, and is more than 2σ deviant in M/L (1.45 for the model population versus 1.89 derived from the dynamics). All the $x = 1.3$ models with massive white dwarfs have such distorted cores that no reasonable fits to $B(r)$ are obtained, as is true for all the $x = 2$ *isotropic* models with the full complement of $1.2M_\odot$ white dwarfs.

The $x = 2$ models with anisotropy are more promising; models 7–9, all with $\xi_t = 15$ and the mass peak at $0.33M_\odot$, all fit reasonably well both to $\sigma(r)$ and $B(r)$. The core fits are somewhat disturbed by the heavy white dwarfs, but not too much so. The "best" one is probably model 8, though that statement reflects aesthetics rather than statistical significance. When the mass peak is moved out to $0.23M_\odot$, $\xi_t = 15$ is too small, and the models become too extended. Isotropic models will fit $B(r)$ if there is not too much mass in heavy remnants, but the velocity fits are very poor. Anisotropic models with $\xi_t = 30$ have better velocity fits, though only one (half 1.2 white dwarfs) gives an acceptable $B(r)$ fit.

The $x = 3$ models only yield fits with isotropic velocity distributions; the number of white dwarfs is sufficiently small that the models are not affected very much by their distribution among mass classes. Such a steep mass function would seem to contradict the star counts, and in any case yields very poor velocity fits.

Thus the dynamics seem to favor a value of x of about 2 and a mildly anisotropic distribution function, with a transition radius of 15–30 core radii. The best velocity dispersion fits come from the smaller value with a mass function peaking at masses somewhat higher than $0.3M_\odot$.

b) The Core and Heavy Remnants

It is clear from the behavior of the core that no more than about 2% of the cluster mass can be in nonluminous stars as heavy as $1.2M_\odot$, and that much is already stretching the uncertainties in the core shape. For remnants more massive yet, the restriction is even more severe. If $x = 2$ or larger, there is no problem, because massive stars were sufficiently rare that neutron stars from stars more massive than $6M_\odot$, say, could still be in the cluster, though even for $x = 2$ black holes from stars more massive than $10M_\odot$, with little or no mass loss, would not be allowed. If x is as small as 1.3, the situation is very severe, and we are allowed only a very small fraction of the heavy remnants ($1.2M_\odot$ white dwarfs and neutron stars) that should have been formed. For x as large as 3, there are no strong constraints.

c) The Outer Envelope and the Form of the Distribution Function near the Cutoff

The tidal cutoff radius of the cluster poses a problem for some of the models. The Roche radius at the present position of the cluster is about 200 pc for a cluster of mass about $6 \times 10^5 M_\odot$, and this is embarrassingly close to the predicted limiting radii of the $\xi_t = 15$ anisotropic model. We do not know, of course, where M3's perigalacticon is or how the Roche radius at perigalacticon is related to the model cutoff, but it would be somewhat surprising if M3 were just at pericenter *now*.

The form of the light distribution at very large radii, however, is very sensitive to the exact form of the energy cutoff in the distribution function, as was shown by King (1966). Relaxation processes in the outer parts have been far too slow to do anything to the stars left over from the initial violent relaxation, so we should not be surprised if the models predict embarrassing behavior at very large radii. In a sense, the rather large amount of effort that has been expended to find the form of the distribution function at high energies resulting from two-body processes has been in vain, because most of the high-energy stars have not had time to participate in such processes. It is not at all clear that other processes inherent in inhomogeneous systems (e.g., evaporation from the core) do not dominate the evolution of the distribution function

at large radii—cf. the papers by Spitzer and collaborators (Spitzer and Shull 1975 and references therein).

The existence of the two high-velocity stars, in fact, indicates that the distribution function is very much more populous near zero energy than the form we have chosen would indicate; the probability of their being unique is very small, and such objects could comprise a large fraction of the population at large radii. Any such modification of the distribution function would increase the need for anisotropy at large radii, since slower cutoffs result in more convex mass distributions (King 1966). The subject is one which we feel is worth pursuing; our numerical scheme is one in which modification of the form of the distribution function is difficult, so we have chosen not to explore the question in detail here.

d) Rotation

It would perhaps be well at this point to make a few comments about rotation. M3 in projection is quite round, which suggests that rotation is not of dynamical importance, but one should check. The question is what rotation law one should look for; solid body rotation over the whole body of the cluster is easy to test for, but the likelihood that the cluster rotates as a solid body is rather small. A linear regression yields a solid-body rotation of 8.3×10^{-4} km s^{-1} arcsec^{-1} in a position angle of 80°, or a maximum rotation velocity of 0.8 km s^{-1} at a radius of 1000 arcsec, the maximum radius to which we have velocity data. The 1σ uncertainty in Ω is 1.6×10^{-3}, so the solid body rotation is neither important dynamically nor statistically significantly present. We will show in a subsequent paper that a simple class of dynamical models with rotation predicts a rotation angular velocity that is proportional to the square of the tangential velocity dispersion in the cluster, so that the central regions rotate as a solid body but the rotation falls to zero as one approaches the boundary. The fits to such a rotation law depend a bit on the cluster model but typically yield a central value of Ω of about 2.8×10^{-3} km s^{-1} arcsec^{-1}, with the axis in a position angle of about 110°. The maximum rotation velocity is about 1 km s^{-1} at about 30 core radii, and again the rotation is not dynamically important, though it is probably real.

e) Anisotropy

We have seen that the best fitting models are anisotropic with transition radii at about 15 core radii; needed modifications to the high-energy end of the distribution function should make the transition radius even somewhat smaller. The deflection relaxation time for model 8 is equal to the Hubble time at about 6 core radii. The relaxation time at 15 core radii is about an order of magnitude longer. We have argued that the decay of anisotropy at a given radius is influenced mostly by the value of t_d near that radius, but without detailed calculations it is not clear whether relaxation processes at $5r_c$ can *determine* anisotropy at $15r_c$. It is clear in any case that the anisotropy radius could not be very much smaller than it is without conflicting with the cluster age.

f) Relaxation

The central relaxation time [cf. Eq. (38)] is about 1.0×10^8 yr for model 8. (It is somewhat shorter for models with a full complement of $1.2M_\odot$ white dwarfs and flatter mass functions, but those models do not fit well.) The half-mass reference relaxation time t_{rh} defined by Spitzer and his collaborators (see, e.g., Spitzer and Shull 1975, Lightman and Shapiro 1978), is 1×10^{10} yr. (The half-mass radius is about 17 pc.) Since core collapse and evaporation occur on a time scale of several t_{rh}, one expects no significant consequence of these processes on M3 as it is at present. It is not clear whether the mass function we have adopted is subject to the Spitzer segregation instability (Spitzer 1969), but if it is even that relatively rapid process probably has not had time to proceed far. The relaxation time is short enough that the assumption of thermal equilibrium (if there is no instability) is probably a good one, at least for the inner half of the mass. The density-averaged relaxation times defined in Eq. (37) are shorter than the Hubble time for the first three mass classes; the times for mass classes 4–7 are 2.5×10^{10}, 6.3×10^{10}, 1.3×10^{11}, and 2.4×10^{11} years, respectively.

These increasing times mostly reflect the relative avoidance of the core by these light stars. The distribution in the outer parts is not very different, as is shown in Fig. 9, where the projected density profiles are shown for model 8 for several mass classes. It is interesting that in the outer parts the velocity dispersions of all the mass classes is very nearly the same; at 30 core radii, for example, that for class 7 ($0.13M_\odot$) is only 15% larger than that for the giants. Thus the cluster dynamics in the outer part is very much the same, whether one assumes complete thermal equilibrium or only the velocity relaxation expected from the initial violent processes.

IX. CONCLUSIONS AND SUMMARY

We have measured the velocities of 111 stars in the globular cluster M3, with characteristic accuracy ~1 km s^{-1}. These data, as we have seen, are consistent with the absence of spectroscopic binaries in the cluster, but probably require stochastic atmospheric motions of a fraction of a kilometer per second for their successful interpretation. Two stars of variable velocity are known pulsating variable stars; two other stars of constant velocity stand 3.5 and 4.5 times the cluster velocity dispersion from the mean and are considered separately in the analysis.

We have adopted an age of 15×10^9 yr, a helium abundance Y of 0.25, and a modulus of 15.08, based mostly on evolutionary models by Ciardullo and De-

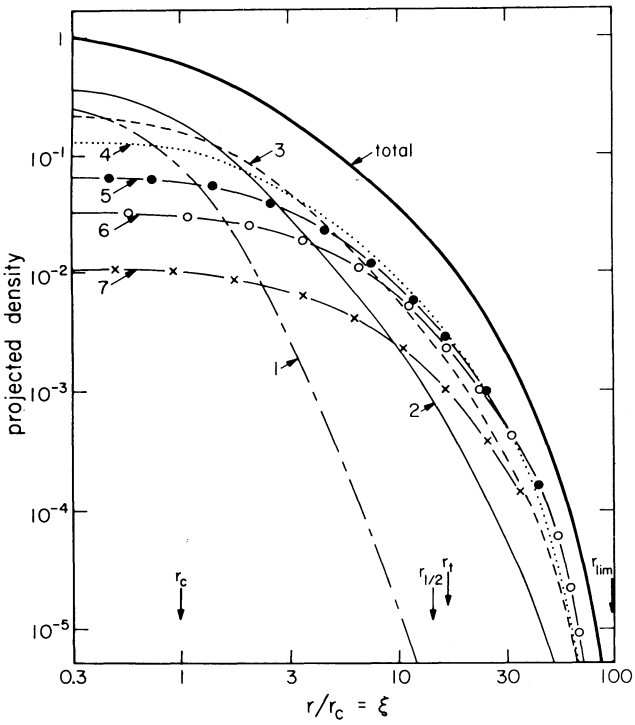

FIG. 9. The projected densities for each of the mass classes in model 8.

marque (1977) and atmospheres and synthetic colors by Böhm-Vitense (1973). The Sandage (1957) counts, interpreted in the context of these same models, yield a main-sequence luminosity function slope x of about 2.0, a value which is supported by the dynamical models.

"Thermal equilibrium" models of the King–Mitchie type have been constructed, which successfully represent the observed light distribution, fit the input mass-to-light ratio, and fit the run of velocity dispersion with radius. The models which fit best have a few remnants (probably white dwarfs) heavier than the current giant mass ($\sim 0.79 M_\odot$), but a limit of about 2% of the cluster mass can be in such objects, and that limit goes down as the mass of the remnants goes up. (We assumed $1.2 M_\odot$ for their mass.) The extremely low radial-velocity dispersion in the outermost parts of the cluster requires that the velocity distribution function become anisotropic there; the transition radius is probably about 15 core radii.

The existence of two high-energy stars indicates that we have imposed too rapid an energy cutoff in our assumed form for the distribution function. The existence of these stars and the concomitant slow energy cutoff pose something of a puzzle, since the frictional slowing-down times are embarrassingly short for such stars, and there is no reasonable mechanism for producing such high-energy objects by diffusion or by binary encounters.

It is perhaps important that models *can* be constructed that have simple dynamics and fit all the observed parameters quite well without appeal to any "missing mass" or any *ad hoc* species other than white dwarfs. These one expects as a result of evolution from a mass function that is consistent with the one indicated for the present main sequence.

The mass function we derive is similar to the one found by Schmidt (1975) for the high-velocity stars in the Galaxy, and it is tempting to say that the population II mass function is probably steeper than the one in the disk. On the other hand, Da Costa (as reported by Freeman 1977) has shown that in four nearby southern clusters, the mass functions are quite different, with x ranging from ~ 0 to ~ 3. Both he and Illingworth and King (1977), in considering dynamical core models based on central velocity dispersions, found that more white dwarfs or other dark objects of similar mass were required to fit the derived core mass-to-light ratios than could be produced by even the flat mass functions assumed. A steeper mass function would help that situation, since the missing white dwarfs of $0.4 M_\odot$–$0.6 M_\odot$ are partly replaced by faint main-sequence stars in the same mass range, though there are, of course, even fewer white dwarfs predicted. It is doubtful whether the discrepancy can be removed, but in some cases the small value of x seems quite certain from direct observation. There seems little doubt that the mass functions do vary; whether or not some clusters have "missing mass" remains for more detailed dynamical study to ascertain, but M3 apparently does not.

A number of problems remain, which can reasonably be answered by other observations and more astute theoretical work. A great deal of recent work on the evolution of clusters via two-body relaxation casts doubt on the applicability of the thermal equilibrium models used here. [See the excellent recent review by Lightman and Shapiro (1978).] One great failing of the work done so far is that *stellar* evolution, with the evolution downward of the mean mass per star, has not been considered and may well dominate, or at any rate drastically modify, the course of such evolution. Our mass function is, of course, amenable to direct confirmation; counts to $V = 26$ can probably be made from the ground with large telescopes and CCDs; this corresponds to $M_V = 11$, or a mass of $0.3 M_\odot$. The space telescope should do about a magnitude or perhaps even two better yet.

Our results on anisotropy and its probable presence seem at variance with those of Cudworth (1976) for another cluster from proper motions; our inferences are quite indirect, of course, and his (in principle) quite direct, though the problem is very difficult. It is possible that M92 is isotropic and M3 not, but that seems unlikely, especially since M3 is, according to our results, almost maximally anisotropic consistent with the deflection relaxation rates.

The authors would like to thank Gary Tuton and Juan Carrasco for expert assistance at the telescope, Earle Emery for perennial patience and help in constructing many last-minute gadgets for the spectrometer, Barbara

Zimmerman for assistance with the analysis software, and many colleagues (especially Lyman Spitzer, Martin Schwarzschild, Donald Lynden-Bell, and Ivan King) for (usually) gentle nagging about publishing these data over the last six years. JEG acknowledges the kind hospitality of the Cambridge University Institute of Astronomy and the University of Chicago, where the models were developed and much of the data analysis was done. This research was supported in part by the U.S. National Science Foundation through grants AST76-80801 A01 and AST76-22111, the Gould fund of the National Academy of Sciences, the Science Research Council of the United Kingdom, and the Alfred P. Sloan Foundation through a fellowship to one of us (JEG).

REFERENCES

Babcock, H. W. (1971). Ann. Rep., Director, Hale Obs., p. 413.
Bailey, S. I. (1913). Ann. Harvard Coll. Obs. **78,** 1.
Barnard, E. E. (1906). Astron. Nachr. **172,** 345.
Barnard, E. E. (1931). Yerkes Publ. **6,** 44.
Baum, W. A. (1952). Astron. J. **57,** 222.
Böhm-Vitense, E., and Szkody, P. (1973). Astrophys. J. **184,** 211.
Böhm-Vitense, E. (1973). Astron. Astrophys. **24,** 447.
Burr, I. W. (1974). *Applied Statistical Methods* (Academic, New York).
Camm, G. L. (1952). Mon. Not. R. Astron. Soc. **112,** 155.
Ciardullo, R., and Demarque, P. (1977). Trans. Astron. Obs. Yale U. 33, 1.
Cudworth, K. (1976). J. Astron. **81,** 975.
Copeland, H., Jensen, J. O., and Jørgensen, H. E. (1970). Astron. Astrophys. **5,** 12.
Da Costa, G. S., and Freeman, K. C. (1976). Astrophys. J. **206,** 128.
Da Costa, G. S., Freeman, K. C., Kalnajs, A. J., Rodgers, A. W., and Stapinski, T. E. (1977). Astron. J. **82,** 810.
Feast, M. W., and Thackeray, A. D. (1960). Mon. Not. R. Astron. Soc. **120,** 463.
Freeman, K. C. (1977). In *The Evolution of Galaxies and Stellar Populations* (Yale U. Obs., New Haven, CT), p. 133.
Griffin, R. F. (1967). Astrophys. J. **148,** 465.
Griffin, R. F., and Gunn, J. E. (1974). Astrophys. J. **191,** 545.
Harding, G. A. (1965). R. Obs. Bull. No. 99.
Heard, J. F. (1956). Publ. David Dunlap Obs. **2,** 107.
Hills, J. G. (1975). Astron. J. **80,** 809.
Illingworth, G. (1976). Astrophys. J. **204,** 73.
Illingworth, G., and King, I. (1977). Astrophys. J. Lett. 218, L109.
Jeans, J. H. (1916). Mon. Not. R. Astron. Soc. **76,** 5.
Joy, A. H. (1940). Astrophys. J. **92,** 396.
Joy, A. H. (1949). Astrophys. J. **110,** 105.
King, I. R. (1962). Astron. J. **67,** 471.
King, I. R. (1965). Astron. J. **70,** 376.
King, I. R. (1966). Astron. J. **71,** 64.
Lightman, A. P., and Shapiro, S. L. (1978). Rev. Mod. Phys. **50,** 437.
Lohmann, W. (1963). Z. Astrophys. **57,** 288.
Lohmann, W. (1975). Astrophys. Space Sci. **32,** 153.
Mitchie, R. W. (1963). Mon. Not. R. Astron. Soc. **125,** 127.
Mitchie, R. W., and Bodenheimer, P. (1963). Mon. Not. R. Astron. Soc. **126,** 269.
Oort, J. H., and van Herk, G. (1959). Bull. Astron. Inst. Neth. **14,** 299.
Ostriker, J. P., Spitzer, L., and Chevalier, R. A. (1972). Astrophys. J. Lett. **176,** L51.
Petersen, C. J., and King, I. R. (1975). Astron. J. **80,** 427.
Pickering, E. C. (1897). Harvard Ann. **26,** 231.
Plummer, H. C. (1911). Mon. Not. R. Astron. Soc. **71,** 460.
Plummer, H. C. (1915). Mon. Not. R. Astron. Soc. **76,** 107.
Popper, D. M. (1947). Astrophys. J. **105,** 211.
Roman, N. G. (1955). Astrophys. J. Suppl. **2,** 195.
Sandage, A. R. (1953). Astron. J. **58,** 61.
Sandage, A. R. (1957). Astrophys. J. **125,** 422.
Sandage, A. R. (1970). Astrophys. J. **162,** 841.
Schmidt, M. (1975). Astrophys. J. **202,** 22.
Spitzer, L. (1940). Mon. Not. R. Astron. Soc. **100,** 396.
Spitzer, L. (1962). *The Physics of Ionized Gases* (Wiley, New York).
Spitzer, L. (1969). Astrophys. J. Lett. **158,** L139.
Spitzer, L., and Härm, R. (1958). Astrophys. J. **127,** 544.
Spitzer, L., and Shull, J. M. (1975). Astrophys. J. **201,** 773.
Veeder, G. (1974). Astron. J. **79,** 1056.
Von Hoerner, S. (1957). Astrophys. J. **125,** 451.
von Zeipel, M. H. (1908). Ann. Obs. Paris **25,** F1.
Wilson, O. C., and Coffeen, M. F. (1954). Astrophys. J. **119,** 197.
Woolley, R. v.d.R. (1954). Mon. Not. R. Astron. Soc. **114,** 191.
Woolley, R. v.d.R., and Robertson, D. A. (1956). Mon. Not. R. Astron. Soc. **116,** 288.
Woolley, R. v.d.R., and Dickens, R. J. (1961). R. Obs. Bull. No. 46.
Woolley, R. v.d.R., and Dickens, R. J. (1962). R. Obs. Bull. No. 54.